
SCIENCE-T2I: Addressing Scientific Illusions in Image Synthesis

Jialuo Li¹ Wenhao Chai² Xingyu Fu³ Haiyang Xu⁴ Saining Xie¹

¹New York University ²University of Washington
³University of Pennsylvania ⁴University of California, San Diego

Abstract

Current image generation models produce visually compelling but scientifically implausible images, exposing a fundamental gap between visual fidelity and physical realism. In this work, we introduce SCIENCE-T2I, an expert-annotated dataset comprising a training set of over 20k adversarial image pairs and 9k prompts across 16 scientific domains and an isolated test set of 454 challenging prompts. Using this benchmark, we evaluate 18 recent image generation models and find that none scores above 50 out of 100 under implicit scientific prompts, while explicit prompts that directly describe the intended outcome yield scores roughly 35 points higher, confirming that current models can render correct scenes when told what to depict but cannot reason from scientific cues to the correct visual outcome. To address this, we develop SciSCORE, a reward model fine-tuned from CLIP-H that captures fine-grained scientific phenomena without relying on language-guided inference, surpassing GPT-4o and experienced human evaluators by roughly 5 points. We further propose a two-stage alignment framework combining supervised fine-tuning with masked online fine-tuning to inject scientific knowledge into generative models. Applying this framework to FLUX.1[dev] yields a relative improvement exceeding 50% on SciSCORE, demonstrating that scientific reasoning in image generation can be substantially improved through targeted data and alignment.

	Website	https://jialuo-li.github.io/Science-T2I-Web/
	Code	https://github.com/Jialuo-Li/Science-T2I
	Data	https://huggingface.co/datasets/Jialuo21/science-t2i
	Model	https://huggingface.co/Jialuo21/Science-T2I-Flux-SFT-OFT

1 Introduction

The quest to conceptualize the visual world and construct real world simulators has been a longstanding endeavor in the computer vision community [1–6]. As articulated by [7], “The goal of image synthesis is to create, using the computer, a visual experience that is identical to what a viewer would experience when viewing a real environment.” In alignment with this vision, recent advances in generative modeling have notably improved the performance of image synthesis [8–13]. While these advancements enable the generation of higher resolution, more aesthetically pleasing images with superior Fréchet Inception Distance (FID) scores [8, 14–16], these models often produce superficial imitations rather than authentic representations of the real visual world [17–20]. This limitation often arises from an inadequate understanding of the underlying scientific principles of realism, as demonstrated in the lower row of FLUX [14] generated images in Figure 1. Consequently, the images generated tend to mirror imaginative constructs, resulting in a noticeable gap between these creations and the tangible reality we inhabit.

To bridge this gap between visual imagination and scientific realism, we introduce SCIENCE-T2I, an expert-annotated dataset partitioned into two isolated components: (1) a training set of over 20k adversarial image pairs and 9k prompts

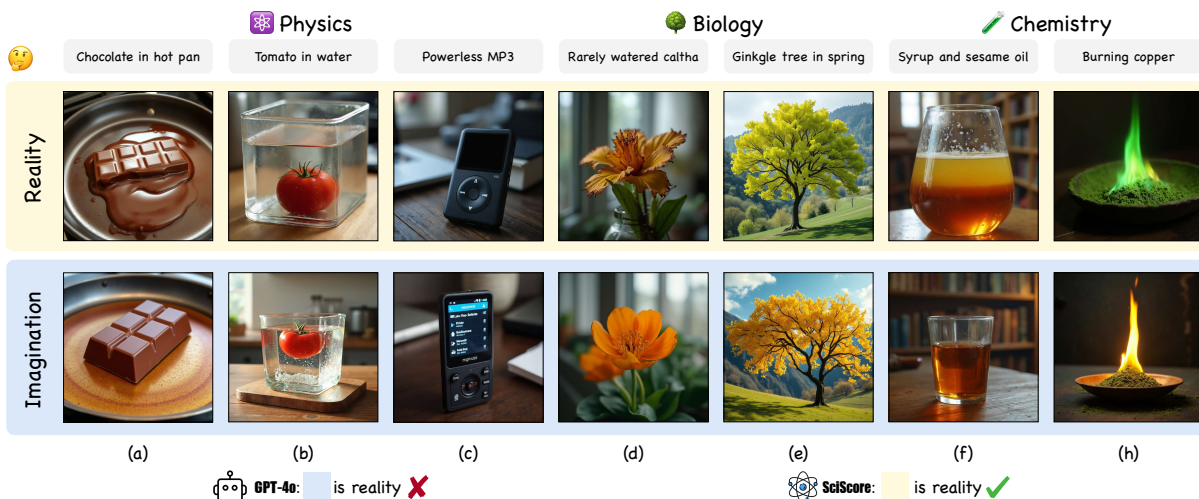


Figure 1: Comparison between GPT-4o and SciScore. Given a prompt (in grey) requiring scientific knowledge, FLUX [14] model generates imaginary images (lower row) that are far from reality (upper row). Moreover, LMMs like GPT-4o [21] fail to identify the realistic image, whereas our reward model SciScore succeeds. Notice that the prompts here are summaries of the real prompts that we used for illustration purposes.

spanning 16 scientific domains across physics, chemistry, and biology, where each pair contrasts a scientifically accurate image with a flawed counterpart to facilitate preference modeling; and (2) a test set of 454 challenging prompts designed to benchmark the scientific plausibility of contemporary image generation models. All data across both splits underwent rigorous validation by human domain experts.

Using this test set, we conduct a systematic evaluation of 18 recent image generation models and find that none achieves a score above 50 out of 100 under implicit prompts. When the same models are evaluated with explicit prompts that directly describe the intended scientific outcome, scores increase by roughly 35 points on average. This gap reveals that current models can render scientifically correct scenes when explicitly instructed, yet cannot reason from implicit scientific cues to the correct visual outcome.

Leveraging the SCIENCE-T2I training set, we develop SciScore, a reward model that extends CLIP-H [22] with scientific knowledge to assess whether generated images faithfully reflect the physical principles implied by a prompt. We find that SciScore outperforms large multimodal models (LMMs) such as GPT-4o [21] on this task: while LMMs often overlook fine-grained visual cues, as shown in Figure 1, SciScore captures them reliably without requiring language-guided inference.

Building upon SciScore, we propose a two-stage alignment framework to inject scientific knowledge into generative models. We first apply supervised fine-tuning (SFT) on FLUX.1[dev] [14] using the SCIENCE-T2I training set, then perform online fine-tuning (OFT) with SciScore as the reward signal and a subject-based masking strategy to stabilize optimization. Our contributions are as follows:

- We introduce SCIENCE-T2I, comprising over 20k expert-annotated adversarial pairs for preference alignment and 454 isolated test prompts for benchmarking the scientific realism of image generation models.
- Using this benchmark, we evaluate 18 image generation models and find that all score below 50 under implicit prompts, with an average 35-point gap compared to explicit prompts, exposing a systematic lack of scientific reasoning in current systems.
- We develop SciScore, a reward model that captures subtle scientific phenomena, surpassing state-of-the-art LMMs and human evaluators on our benchmark.
- We propose a two-stage alignment framework that improves FLUX.1[dev] [14] by over 50% on SciScore, demonstrating that scientific reasoning in image generation can be substantially enhanced through targeted data and alignment.

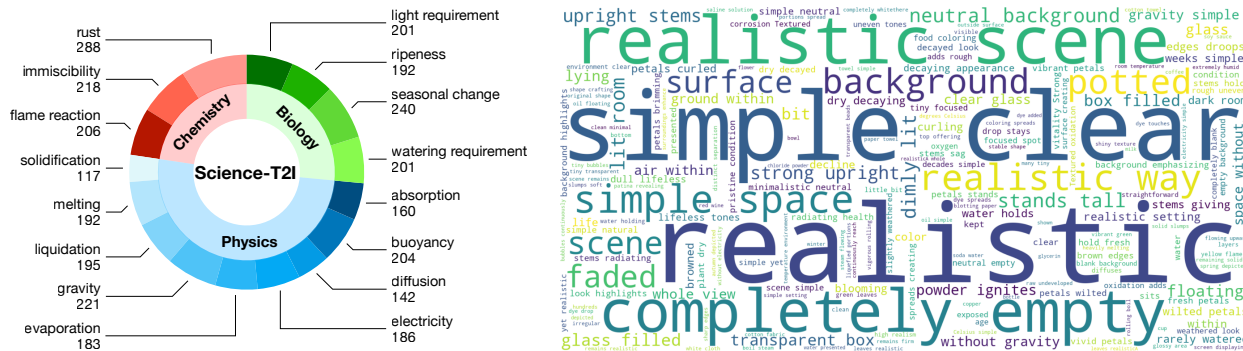


Figure 2: Data statistics. (Left) SCIENCE-T2I is organized into three primary scientific fields: Chemistry, Biology, and Physics. Each field is divided into specific categories, with the numbers indicating the volume of implicit prompts collected for each category. (Right) Word cloud of structured prompts in SCIENCE-T2I.

2 SCIENCE-T2I: Bridging Visual Imagination and Scientific Realism

As established above, current image generation models produce visually plausible but scientifically incorrect outputs when prompted with descriptions that require physical reasoning. We identify two root causes: (1) existing training data rarely pairs scientific concepts with their correct visual manifestations, and (2) standard evaluation protocols do not test whether a model understands the science behind a prompt or merely matches its surface-level descriptions. To address both issues, we introduce SCIENCE-T2I, a dataset that challenges models to perform implicit reasoning rather than textual rendering. Unlike conventional datasets that focus on textual descriptions [23–25] or preferences [26–28], SCIENCE-T2I requires models to infer visual outcomes from prompts grounded in scientific principles.

Task overview. As illustrated in Figure 2, SCIENCE-T2I consists of 16 tasks spanning physics, chemistry, and biology. Each task requires the model to infer or visualize a concept not explicitly stated in the prompt but rooted in an underlying scientific principle. These tasks draw on existing research such as PhyBench [17] and Commonsense-T2I [18], and extend them with new phenomena developed for this study. Each task satisfies two design objectives:

- **Rewriting Capability.** Prompts allow flexible rephrasing while preserving the same visual meaning. For example, *an unripe apple* can be rephrased as *a green apple*, conveying an identical visual concept. This property enables the construction of explicit and superficial prompt variants from a single implicit prompt, as described below. Further explanations and examples are provided in Appendix A.
- **Scientific Knowledge Integration.** Tasks are grounded in established scientific principles, providing a clear and consistent framework. Compared to commonsense knowledge, which can vary culturally or contextually, scientific principles offer unambiguous ground truth for evaluating correctness.

Detailed descriptions of all 16 tasks are provided in Appendix B. Beyond the classification by scientific discipline, we observe that the tasks naturally fall into two categories that reveal distinct reasoning demands:

- **Subject-oriented Tasks (ST)** require reasoning about how inherent differences between subjects lead to varying visual features under identical conditions. For example, different metals produce different flame colors.
- **Condition-oriented Tasks (CT)** focus on how a single condition affects the visual appearance of various subjects. Here, scientific reasoning centers on the applied condition rather than the subject’s individual properties. For example, all objects float in the absence of gravity.

As we show in Section 4.4, this distinction proves analytically useful: nearly all failure cases of SciSCORE concentrate in ST, where subject-specific knowledge is required rather than generalizable visual patterns. The full classification of each task is provided in Appendix C.

Prompt design. A central design choice in SCIENCE-T2I is the three-tier prompt structure, which disentangles a model’s scientific reasoning ability from its compositional rendering ability. Prior work [17] observes that models often ignore implicit scientific cues and attend only to surface-level text, motivating us to introduce a third prompt type that captures this failure mode. For each task, we construct a tuple of three prompts:

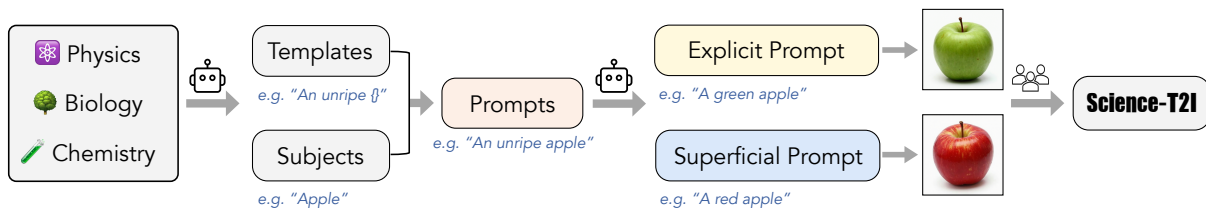


Figure 3: Data curation pipeline. For each task, GPT-4o [21] first generates structured templates that capture the scientific principles while allowing for variability in objects or substances. These templates are used to create implicit prompts, which GPT-4o [21] then expands into explicit and superficial prompts, ultimately guiding the synthesis of corresponding explicit and superficial images.

- **Implicit Prompt (IP)** contains terms that imply certain visual characteristics requiring interpretative reasoning based on scientific knowledge. For example, “an unripe apple” suggests greenness without explicitly stating it.
- **Explicit Prompt (EP)** reformulates the implicit prompt into a clear, descriptive statement that directly conveys the intended visual outcome. For instance, “a green apple” makes the expected appearance explicit.
- **Superficial Prompt (SP)** provides a plausible but scientifically incorrect interpretation of the implicit prompt, focusing only on surface-level associations. For example, “a red apple” interprets “unripe” based on the default visual prototype rather than the scientific implication.

Together, the three prompt types serve complementary roles: the IP tests implicit reasoning, the EP establishes an upper bound on what the model can render when given direct instructions, and the SP provides a hard negative for preference-based training. Each training tuple in SCIENCE-T2I pairs these prompts with corresponding explicit and superficial images, forming the adversarial format required for reward modeling (Section 4.2).

Data curation. We leverage GPT-4o [21] to generate structured templates and corresponding prompts for each task. As illustrated in Figure 3, the pipeline first produces implicit prompts from task-specific templates, then expands each implicit prompt into its explicit and superficial counterparts. These prompts are used to generate image pairs via image generation models. To ensure quality, all generated data undergoes manual verification by domain experts, who cross-reference each tuple against established scientific knowledge. Further details are provided in Appendix D.

3 Benchmarking Scientific Image Synthesis

Having introduced the SCIENCE-T2I training set and its prompt structure, we now turn to evaluation. We construct a dedicated test set, define a two-tiered grading framework, and use it to benchmark recent image generation models. The results expose a systematic gap between compositional rendering and scientific reasoning.

Test splits. We construct two manually annotated test sets covering the same scientific domains as the training data but containing no overlapping samples. Each tuple is reviewed iteratively by domain experts who cross-reference their annotations with authoritative scientific sources until unanimous consensus is reached. To evaluate generation quality under varying visual complexity, we split the benchmark into two subsets:

- **SCIENCE-T2I-S (Simple)**, containing 227 tuples. This split uses minimalist compositions with simple backgrounds. By isolating the scientific subject from environmental distractions, it provides a controlled test of whether the model can generate the correct scientific visual features.
- **SCIENCE-T2I-C (Complex)**, containing 227 tuples. This split embeds the same scientific tasks within diverse real-world scenes, adding contextual elements such as “in a bedroom” or “on the street.” It tests a more challenging setting: whether the model can maintain scientific accuracy when the background is visually complex and potentially distracting. Strong performance on SCIENCE-T2I-C indicates generalization beyond the training distribution.

For brevity, we refer to the union of both splits as the SCIENCE-T2I test set below.

Grading criteria. We leverage the vision and reasoning capabilities of LMMs to assess generated images. To ensure reliable and fine-grained evaluation, we develop per-tuple grading criteria inspired by PhyBench [17]. Each tuple is scored along two complementary aspects:

Table 1: Current image generation models struggle with implicit scientific reasoning across all domains. We evaluate 18 models on SCIENCE-T2I using implicit prompts and report the normalized Reality Score evaluated by Qwen3.5-27B [29] for Physics, Chemistry, and Biology. Even the strongest model scores below 50, and Biology consistently lags behind the other two domains. **Bold** and underlined denote the best and second-best results.

Model	SCIENCE-T2I			
	Physics	Chemistry	Biology	Overall
SDXL [8]	16.11	20.92	25.56	19.60
FLUX.1[schnell] [14]	23.19	38.30	13.33	23.72
LongCat-Image [30]	21.94	39.01	15.83	23.86
GLM-Image [31]	22.22	41.84	14.44	24.23
SANA [32]	23.89	46.45	14.72	26.14
Lumina-Image-2 [33]	20.28	47.87	22.22	26.51
SD 3.5 Medium [34]	23.06	39.01	24.44	26.73
Z-Image [35]	26.53	32.98	22.22	26.73
FLUX.1[dev] [14]	22.64	50.00	17.22	26.87
SD 3.5 Large [34]	27.64	44.68	18.33	28.71
Bagel [36]	25.28	45.75	23.33	29.00
FLUX.2[klein-4B-Base] [37]	27.22	43.97	21.11	29.08
Z-Image-Turbo [35]	26.81	36.53	<u>28.33</u>	29.22
FLUX.2[klein-4B] [37]	28.75	50.36	19.72	30.84
FLUX.2[klein-9B-Base] [37]	30.28	45.75	23.06	31.57
FLUX.2[klein-9B] [37]	29.44	57.45	19.44	32.60
Qwen-Image [38]	<u>34.58</u>	46.45	23.06	<u>33.99</u>
FLUX.2[dev] [37]	53.19	<u>53.55</u>	32.50	47.80

- **Scene Score (SS)** measures whether all descriptive visual content specified in the prompt is faithfully present in the generated image. The full score is 2.
- **Reality Score (RS)** assesses whether the implicit visual elements, derived from the underlying scientific principles, are accurately depicted in the image. The full score is 3.

We present representative examples of the grading criteria and corresponding prompts in Figure 16.

Scoring protocol. For each tuple in the SCIENCE-T2I test set, we use the implicit prompt to generate two images with each model. We then employ Qwen3.5-27B [29] as the evaluator following the instruction template detailed in Figure 17. For every generated image, Qwen3.5-27B [29] receives the image alongside the implicit prompt and its grading criteria, and produces its SS and RS scores. Notably, within this two-tiered framework, assessing scientific correctness is meaningful only when the main subject is correctly depicted. We therefore set RS to zero for any image that does not achieve a full SS. To obtain the final metric, we normalize the RS to the range of [0, 100].

Models. We evaluate 18 image generation models spanning diverse architectures and scales. These include the Stable Diffusion series [8, 34], the FLUX series [14], and recent models such as GLM-Image [31], Qwen-Image [38], Z-Image [35], Bagel [36], SANA [32], Lumina-Image-2 [33], and LongCat-Image [30]. This selection covers both open-source and proprietary systems released between 2022 and 2025, providing a representative snapshot of current capabilities. The full results are presented in Table 1.

Current models lack scientific image synthesis capabilities. As shown in Table 1, all 18 models exhibit consistently low scores on SCIENCE-T2I under implicit prompts. Even the best-performing model, FLUX.2[dev] [37], achieves only 47.80 out of 100, and the majority of models cluster between 20 and 35. Among the three domains, Biology poses the greatest challenge: no model exceeds 33%, suggesting that biological reasoning remains particularly underrepresented in current training data. A telling example is Z-Image [35], a model widely recognized for its photorealistic quality and strong compositional capabilities. Despite being a recent and highly competitive model, it scores only 26.73 on SCIENCE-T2I, lower than the significantly earlier FLUX.1[dev] [14] at 26.87. This observation

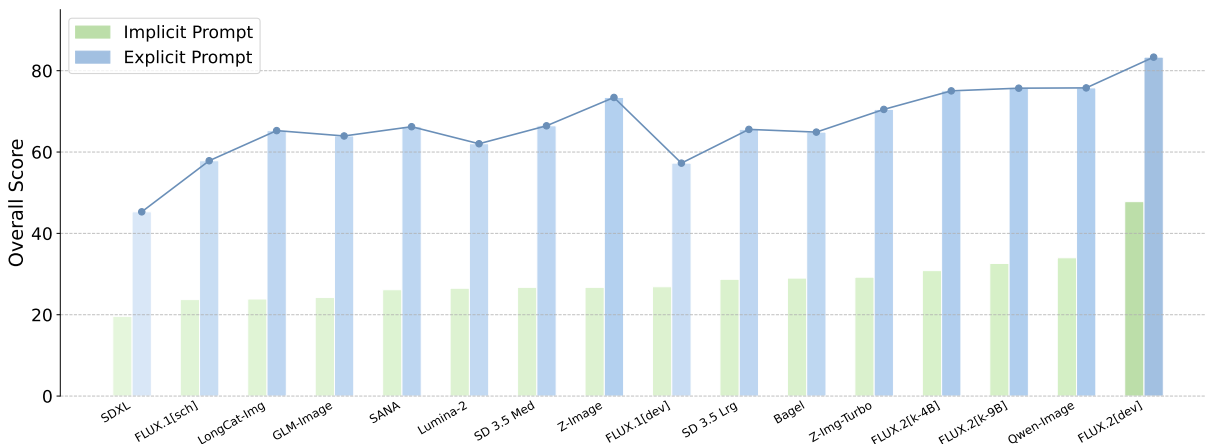


Figure 4: Explicit prompts close the gap that implicit prompts expose. All models score significantly higher under explicit prompts (blue) than implicit prompts (green), with an average gap of roughly 35 points. The trend line highlights that even as overall capability increases, the composition–reasoning disconnect persists across all models.

indicates that advances in visual fidelity and scene composition do not translate into scientific reasoning ability, and that current training pipelines systematically lack data targeting this capability.

Explicit prompts reveal a composition–reasoning disconnect. The results above show that models perform poorly under implicit prompts, but they do not reveal whether the bottleneck lies in visual rendering or in scientific reasoning. To disentangle these two factors, we replace each implicit prompt with its corresponding explicit prompt and re-evaluate all models using Qwen3.5-27B [29]. The results, shown in Figure 4, reveal a striking gap: across all 18 models, explicit prompts yield scores roughly 35 points higher than implicit prompts on average. This demonstrates that current models can faithfully render scientifically correct scenes when explicitly told what to depict, yet fail to infer the same visual outcome from implicit scientific cues. The contrast is especially pronounced for Z-Image [35], which achieves 73.42 under explicit prompts but only 26.73 under implicit prompts, a gap of nearly 47 points. This finding clarifies that the bottleneck is not in visual rendering but in scientific reasoning: models excel at translating direct descriptions into images, but lack the capacity to reason from scientific principles to their visual consequences.

4 SciScore: A Reward Model Grounded in Reality

CLIP [39] aligns textual and visual data effectively for general purposes, but we find that it struggles with implicit scientific prompts: it tends to embed implicit prompts closer to their superficial counterparts than their explicit counterparts, because surface-level associations dominate over scientific implications. To address this, we introduce SciScore, a reward model fine-tuned on the SCIENCE-T2I training set that extends CLIP to assess whether a generated image reflects the scientific principles implied by a prompt. We first define the reward formulation (§4.1) and then describe the two training objectives that jointly optimize SciScore (§4.2).

4.1 Reward Formulation

SciScore builds on the CLIP architecture [39], encoding a text prompt x and an image y into a shared high-dimensional space using separate transformer encoders [40], E_{txt} and E_{img} . The reward is the cosine similarity between the two representations, scaled by a learnable temperature T :

$$r(y, x) = T \cdot \frac{E_{\text{txt}}(x) \cdot E_{\text{img}}(y)}{\|E_{\text{txt}}(x)\| \|E_{\text{img}}(y)\|}. \quad (1)$$

4.2 Training Objective

We fine-tune CLIP-H [22] on the SCIENCE-T2I training set with both encoders learnable. Each training instance is a tuple $(x_i, x_e, x_s, y_e, y_s)$: an implicit prompt x_i , its explicit and superficial counterparts x_e and x_s , and the corresponding explicit and superficial images y_e and y_s . The training objective combines two complementary losses targeting the text and image encoders, respectively.

Preference formulation. Following preference modeling in language [41, 42], the predicted preference $\hat{p}_{\text{img}}(x_a \succ x_b; y)$ for prompt x_a over prompt x_b for a given image y is calculated as:

$$\hat{p}_{\text{img}}(x_a \succ x_b; y) = \frac{\exp(r(y, x_a))}{\exp(r(y, x_b)) + \exp(r(y, x_a))} \quad (2)$$

Similarly, for a given prompt x , the predicted preference $\hat{p}_{\text{txt}}(y_a \succ y_b; x)$ for image y_a over image y_b is given by:

$$\hat{p}_{\text{txt}}(y_a \succ y_b; x) = \frac{\exp(r(y_a, x))}{\exp(r(y_a, x)) + \exp(r(y_b, x))} \quad (3)$$

Implicit prompt alignment (IPA). The core challenge is that pretrained CLIP embeds implicit prompts in a manner similar to their superficial counterparts rather than their explicit counterparts, because surface-level co-occurrence patterns dominate over scientific semantics. IPA corrects this by minimizing the KL divergence between the target preference $p_{\text{txt}} = [1, 0]$ and the predicted preference $\hat{p}_{\text{txt}} = [\hat{p}_{\text{txt}}(y_e \succ y_s; x_i), \hat{p}_{\text{txt}}(y_s \succ y_e; x_i)]$, effectively steering the implicit prompt embedding toward the explicit image:

$$\mathcal{L}_{\text{IPA}} = \sum_{j=1}^2 p_{\text{txt}_j} (\log p_{\text{txt}_j} - \log \hat{p}_{\text{txt}_j}) \quad (4)$$

Image encoder enhancement (IEE). IPA operates exclusively on the text encoder’s representation of the implicit prompt. However, many scientific phenomena manifest as fine-grained visual details (e.g., subtle color differences or layering patterns) that the pretrained image encoder may not attend to. To strengthen the encoder’s sensitivity to these details, we introduce a complementary loss on the image side:

$$\mathcal{L}_{\text{IEE}} = \mathcal{L}_{\text{img}}^+ + \mathcal{L}_{\text{img}}^- \quad (5)$$

where $\mathcal{L}_{\text{img}}^+$ and $\mathcal{L}_{\text{img}}^-$ correspond to the losses associated with explicit and superficial image preferences, respectively. The explicit image loss $\mathcal{L}_{\text{img}}^+$ is defined as:

$$\mathcal{L}_{\text{img}}^+ = \sum_{j=1}^2 p_{\text{img}_j}^+ (\log p_{\text{img}_j}^+ - \log \hat{p}_{\text{img}_j}^+), \quad (6)$$

with $p_{\text{img}}^+ = [1, 0]$ and $\hat{p}_{\text{img}}^+ = [\hat{p}_{\text{img}}(x_e \succ x_s; y_e), \hat{p}_{\text{img}}(x_s \succ x_e; y_e)]$. The superficial image loss is defined symmetrically:

$$\mathcal{L}_{\text{img}}^- = \sum_{j=1}^2 p_{\text{img}_j}^- (\log p_{\text{img}_j}^- - \log \hat{p}_{\text{img}_j}^-), \quad (7)$$

with $p_{\text{img}}^- = [0, 1]$ and $\hat{p}_{\text{img}}^- = [\hat{p}_{\text{img}}(x_e \succ x_s; y_s), \hat{p}_{\text{img}}(x_s \succ x_e; y_s)]$. The overall loss combines both objectives:

$$\mathcal{L} = \mathcal{L}_{\text{IPA}} + \lambda \mathcal{L}_{\text{IEE}}, \quad (8)$$

where λ controls the relative weight of image encoder enhancement. We ablate λ in Section 4.4.

4.3 Experimental Setup

Training and evaluation. We fine-tune CLIP-H [22] on the SCIENCE-T2I training set with both text and image encoders learnable. Training completes within one hour on 8 A6000 GPUs. We evaluate on both SCIENCE-T2I-S and SCIENCE-T2I-C. For detailed configurations, see Appendix F.

Table 2: SciSCORE surpasses all VLMs, LMMs, and human evaluators. Accuracy (%) on the two-choice selection task across Physics, Chemistry, and Biology. Green highlights the best VLM; blue highlights the best LMM.

Model	SCIENCE-T2I-S				SCIENCE-T2I-C			
	Physics	Chemistry	Biology	Avg.	Physics	Chemistry	Biology	Avg.
Human Eval	87.67	75.85	95.29	87.01	84.71	85.40	89.14	86.02
Random Guess	50.00	50.00	50.00	50.00	50.00	50.00	50.00	50.00
CLIP-H [22]	55.08	52.38	55.88	54.69	56.56	44.44	76.67	59.47
BLIPScore [43]	50.35	43.08	59.86	55.00	49.78	60.00	58.33	51.54
SigLIP ViT-SO-14 [45]	59.63	53.17	55.94	57.23	61.48	51.11	70.00	61.67
Qwen2-VL-7B [47]	60.03	67.01	68.82	63.79	66.80	50.00	90.83	69.82
LLaVA-OV-7B [46]	68.22	57.82	64.71	65.05	74.59	50.00	76.67	70.26
InternVL2.5-8B [48]	67.80	62.24	84.41	70.79	73.77	65.56	85.83	75.33
GPT-4o mini [21]	61.97	73.81	86.76	70.83	69.29	70.00	90.00	74.78
GPT-4o mini+ CoT [49]	67.04	76.87	90.00	74.97	72.44	70.00	92.50	77.16
SciSCORE (ours)	94.92	80.95	100.0	93.14	86.89	91.11	100.0	91.19

Baselines. We compare against three categories of baselines: (1) VLMs including CLIP-H [22], BLIPScore [43, 44], and SigLIP [45]; (2) LMMs including LLaVA-OV [46], Qwen2-VL [47], InternVL [48], and GPT-4o-mini [21], with and without CoT [49]; and (3) human evaluations by 10 experts with science or engineering degrees. Details are provided in Appendix G; results are summarized in Table 2.

4.4 SciSCORE Outperforms VLMs, LMMs, and Human Evaluators

VLMs and LMMs fail to distinguish scientifically accurate images. As shown in Table 2, all three VLMs achieve near-random accuracy (54–61%) across both test splits, indicating that general-purpose vision-language alignment provides little signal for scientific reasoning. LMMs fare better but remain far below human performance: even the strongest baseline, GPT-4o-mini with CoT [49], reaches only 74.97 on SCIENCE-T2I-S and 77.16 on SCIENCE-T2I-C, compared to human scores of 87.01 and 86.02. Notably, CoT prompting yields only marginal improvements over the standard GPT-4o-mini, suggesting that the bottleneck lies in visual perception rather than reasoning chain construction. A detailed analysis is provided in Appendix I.

SciSCORE generalizes to complex scenes and surpasses human evaluators. SciSCORE achieves 93.14 on SCIENCE-T2I-S and 91.19 on SCIENCE-T2I-C, surpassing human evaluators (87.01 and 86.02) by roughly 6 and 5 points, respectively. The strong performance on SCIENCE-T2I-C is particularly notable, as this split embeds scientific reasoning tasks within diverse environmental contexts that were not present during training. This suggests that SciSCORE has learned to focus on the scientifically relevant regions of an image while disregarding environmental distractions.

Subject-oriented tasks remain the primary challenge. We further analyze SciSCORE’s performance by the ST/CT classification introduced in Section 2. As shown in Figure 5, nearly all failure cases concentrate in subject-oriented tasks. This is expected: condition-oriented tasks rely on generalizable visual features (e.g., the absence of gravity implies floating objects), whereas subject-oriented tasks demand subject-specific knowledge (e.g., which metals produce which flame colors). For novel or unseen subjects, the model lacks sufficient prior exposure to the subject’s distinctive visual attributes.

$\lambda = 0.25$ balances fine-grained detection with prompt alignment. We ablate the IEE weight λ in Table 3. Setting $\lambda = 0$ disables IEE entirely, yielding optimal performance on SCIENCE-T2I-S but degraded accuracy on SCIENCE-T2I-C, where fine-grained visual discrimination is more critical due to complex backgrounds. Larger values ($\lambda \geq 0.5$) shift too much focus to the image encoder at the expense of prompt alignment. We find that $\lambda = 0.25$ achieves the best balance, matching the top score on both splits simultaneously. Qualitative analysis is provided in Appendix J.

Table 3: $\lambda = 0.25$ achieves the best balance between IPA and IEE. Bold indicates best performance per column.

λ	SCIENCE-T2I-S	SCIENCE-T2I-C
0	93.14	88.99
0.1	92.85	90.75
0.5	92.85	91.19
0.75	93.14	88.99
0.25	93.14	91.19

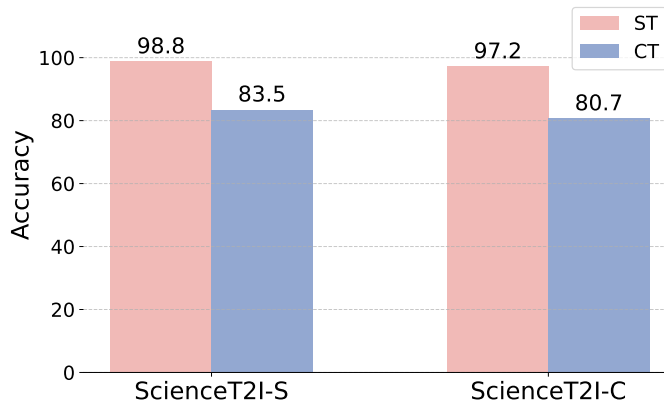


Figure 5: Nearly all SciScore failures concentrate in subject-oriented tasks. Condition-oriented tasks involve generalizable visual patterns and are substantially easier.

5 Aligning Generative Models with Scientific Principles

We now combine the SCIENCE-T2I training set with SciScore as a reward signal to close the reasoning gap identified in Section 3. Our framework proceeds in two stages: SFT exposes the model to scientific visual phenomena it has never encountered during pretraining, and OFT then optimizes for the implicit reasoning ability measured by SciScore.

5.1 SFT Provides the Scientific Knowledge Base

Current post-training algorithms for diffusion models, such as those based on PPO [50, 51] and DPO [16, 52], optimize within the distribution of the pre-trained model. This constraint is acceptable for aesthetic preferences, where the desired outputs already lie within the model’s distribution. However, scientific reasoning presents a fundamentally different challenge: pre-trained models have never been exposed to images depicting scientific phenomena, so no amount of preference optimization over existing outputs can teach them what these phenomena look like. The model must first learn what scientifically correct images are before it can be steered toward generating them.

We therefore begin with supervised fine-tuning on the SCIENCE-T2I training set to provide this missing foundation. Among the models evaluated in Section 3, the FLUX series [14] consistently achieves the strongest text-image alignment and produces the most realistic outputs. We adopt FLUX.1[dev] [14] as our base model. Since FLUX employs the flow matching [53] framework, the SFT objective is:

$$L_{SFT} = \mathbb{E}_{t, p_t(z|\epsilon), p(\epsilon)} \|v_\theta(z, t) - u_t(z|\epsilon)\|_2^2 \quad (9)$$

We adopt the same notation as [34]; further details are provided in Appendix K.

5.2 Online Fine-tuning with SciScore as Reward Signal

SFT teaches the model *what* scientific images look like by training on explicit image pairs. However, it does not directly optimize for the ability to infer the correct visual outcome from an implicit prompt, which is the core capability measured by SciScore. To bridge this remaining gap, we apply online fine-tuning with SciScore as the reward signal, as illustrated in Figure 6. Following DDPO [50], we formulate the denoising process as a multi-step MDP:

$$s_t \triangleq (c, t, x_{1-t}), \pi_\theta(a_t | s_t) \triangleq p_\theta(x_{1-\Delta t-t} | c, t, x_{1-t}), \rho_0(s_0) \triangleq (p(c), \delta_0, \mathcal{N}(0, I)) \quad (10)$$

$$a_t \triangleq x_{1-\Delta t-t}, P(s_{t+\Delta t} | s_t, a_t) \triangleq (\delta_c, \delta_{t+\Delta t}, \delta_{x_{1-t-\Delta t}}), r(s_t, a_t) \triangleq \begin{cases} r(x_0, c) & \text{if } t = 1 \\ 0 & \text{otherwise} \end{cases} \quad (11)$$

We follow the notation of DDPO [50] with minor adjustments to the timestamp convention. However, flow matching [53] is typically formulated as an ODE, yielding a deterministic policy that prevents direct computation of the log-probability required by DPO:

$$\pi_\theta(a_t | s_t) = \delta(x_{1-\Delta t-t} - (x_{1-t} - v_\theta(s_t)\Delta t)) \quad (12)$$

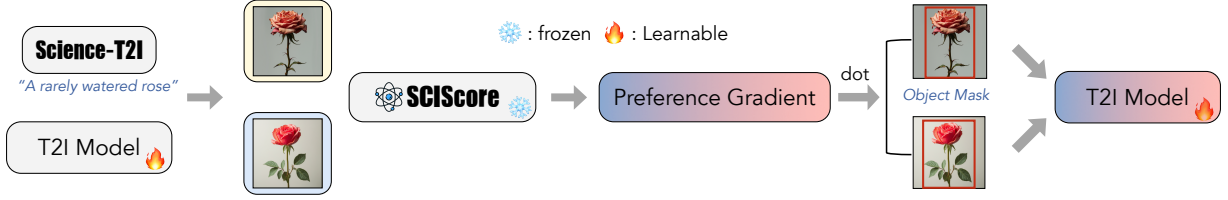


Figure 6: Online fine-tuning uses SciScore and subject-based masking to align generation with scientific principles. For each prompt, two images are generated and scored by SciScore to determine preference. GroundingDINO [56] extracts subject masks from each image, restricting gradient propagation to the relevant regions.

Following [54], we resolve this by interpreting flow matching as an SDE:

$$dx_t = \left(v_\theta(x_t, t) + \frac{\sigma_t^2}{2\beta_t\eta_t} \lambda_t \right) dt + \sigma_t dB_t \quad (13)$$

$$\eta_t = \left(\frac{\dot{\alpha}_t}{\alpha_t} \beta_t - \dot{\beta}_t \right), \quad \lambda_t = \left(v_\theta(x_t, t) - \frac{\dot{\alpha}_t}{\alpha_t} x_t \right) \quad (14)$$

where B_t denotes Brownian motion. Discretizing with the rectified flow used by FLUX [14] ($\alpha_t = t$, $\beta_t = 1 - t$) yields a Gaussian policy:

$$\pi_\theta(a_t | s_t) = \mathcal{N}(a_t; \mu_\theta(s_t), \sigma_t^2 I) \quad (15)$$

$$\mu_\theta(s_t) = \frac{t\sigma_t^2 + 2(1-t)}{-2(1-t)} v_\theta(s_t) \Delta t + \frac{2(1-t) + \sigma_t^2 \Delta t}{2(1-t)} x_{1-t} \quad (16)$$

Setting $\sigma_t = 0$ recovers the deterministic case in Equation 12. For the training objective, we adopt DPO [55], with technical details in Appendix K. Given a prompt c , we sample two denoising trajectories:

$$\sigma_w = \{s_0^w, a_0^w, s_{\Delta t}^w, a_{\Delta t}^w, \dots, s_1^w, a_1^w\}, \quad \sigma_l = \{s_0^l, a_0^l, s_{\Delta t}^l, a_{\Delta t}^l, \dots, s_1^l, a_1^l\} \quad (17)$$

Assuming that the reward satisfies $r(s_1^w, a_1^w) > r(s_1^l, a_1^l)$, the training objective is formulated as:

$$\mathcal{L} = \mathbb{E} \left[\log \rho \left(\beta \log \frac{\pi_\theta(a_k^l | s_k^l)}{\pi_{\text{ref}}(a_k^l | s_k^l)} - \beta \log \frac{\pi_\theta(a_k^w | s_k^w)}{\pi_{\text{ref}}(a_k^w | s_k^w)} \right) \right] \quad (18)$$

Subject-based masking for stable optimization. Without masking, the DPO objective treats all spatial regions of the preferred image as equally desirable. In practice, the preferred and rejected images often differ only in the scientifically relevant region, while sharing similar backgrounds and compositions. Optimizing over the entire image introduces noise from irrelevant features and destabilizes training. To address this, we extract the subject from each prompt and use GroundingDINO [56] to localize it within the generated image. Only the content within the detected bounding box contributes to gradient backpropagation. We define the mask as \mathcal{M} ; the masked objective becomes:

$$\mathcal{L} = -\mathbb{E} \left[\log \rho \left(\beta \log \frac{\mathcal{M}^w \odot \pi_\theta(a_k^w | s_k^w)}{\mathcal{M}^w \odot \pi_{\text{ref}}(a_k^w | s_k^w)} - \beta \log \frac{\mathcal{M}^l \odot \pi_\theta(a_k^l | s_k^l)}{\mathcal{M}^l \odot \pi_{\text{ref}}(a_k^l | s_k^l)} \right) \right].$$

5.3 Training and Evaluation Setup

Training. We first fine-tune FLUX.1[dev] [14] on SCIENCE-T2I using SFT with LoRA [57] for 2,000 steps, producing LoRA weights for the subsequent OFT stage. For OFT, we randomly select 300 implicit prompts from SCIENCE-T2I as the training set. During each epoch, 32 prompts are sampled; for each prompt, two images are generated and scored by SciScore. Subject masks are extracted using GroundingDINO [56]. The model is then fine-tuned for approximately 100 steps. Detailed configurations are provided in Appendix L.

Evaluation. We extract all implicit prompts from SCIENCE-T2I-S and SCIENCE-T2I-C to form two evaluation sets. For each prompt, we generate five images and report the average SciScore to ensure robust results.

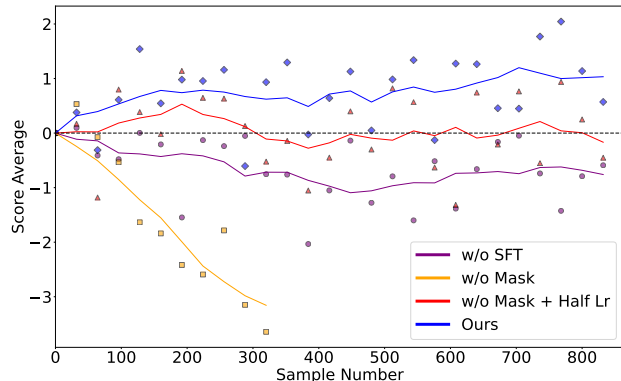


Figure 7: SFT is essential before OFT, and masking stabilizes training. Without prior SFT (purple), OFT fails to improve SciScore. Without masking (yellow/red), performance becomes erratic or stalls.

Table 4: The two-stage framework improves FLUX.1[dev] [14] by over 50% in RI. Bold indicates best performance.

Method	SCIENCE-T2I-S		SCIENCE-T2I-C	
	SciScore	RI	SciScore	RI
FLUX.1[dev] [14]	23.56	/	27.26	/
+EP	32.85	/	34.70	/
+SFT	27.43	41.66	29.49	29.97
+SFT+OFT	28.52	53.39	30.11	38.31

Relative improvement metric. Raw SciScore scores are useful for comparing models but do not reveal how close a fine-tuned model is to its own ceiling. We observe that SciScore under explicit prompts consistently surpasses that under implicit prompts, providing a natural upper bound: the best the model could achieve if it could perfectly reason from implicit cues. To quantify progress toward this ceiling, we define the **Relative Improvement (RI)** metric. Let SciScore_B^{IP} and SciScore_B^{EP} denote the base model’s scores under implicit and explicit prompts, and SciScore_F^{IP} the fine-tuned model’s score under implicit prompts:

$$RI = \frac{\text{SciScore}_F^{IP} - \text{SciScore}_B^{IP}}{\text{SciScore}_B^{EP} - \text{SciScore}_B^{IP}} \quad (19)$$

An RI of 100% would indicate that fine-tuning has fully closed the gap between implicit and explicit prompts.

5.4 Two-Stage Training Yields Over 50% Improvement

SFT and OFT together exceed the baseline by over 50%. Table 4 confirms that both SFT and OFT improve the performance of FLUX [14] on SciScore. The combined two-stage framework increases the score from 23.56 to 28.52 on SCIENCE-T2I-S (RI = 53.39%) and from 27.26 to 30.11 on SCIENCE-T2I-C (RI = 38.31%). We find that SFT contributes the larger share of the improvement, which is expected: SFT provides the foundational knowledge of what scientific images look like, while OFT refines the model’s ability to activate that knowledge from implicit prompts. A qualitative comparison is presented in Figure 8.

The fine-tuned model generalizes to complex scenes. While the SCIENCE-T2I training set primarily contains images in straightforward scenarios, the fine-tuned model shows clear improvement on SCIENCE-T2I-C, which embeds scientific tasks within diverse environmental contexts. This indicates that the model has internalized underlying scientific principles rather than memorizing training examples: the knowledge transfers to visual settings not seen during fine-tuning.

5.5 Both Stages and Masking Are Necessary

We ablate each component to verify that both stages and the masking strategy are necessary. Throughout, we follow a consistent protocol: at each training step, all implicit prompts from SCIENCE-T2I-S are used to generate two images per prompt, and the average SciScore is computed. All curves in Figure 7 show deviations from the baseline.

OFT without preceding SFT fails to improve performance. The blue curve in Figure 7 shows OFT applied after SFT, while the purple curve shows OFT without prior SFT. Both use identical OFT configurations. We find that SFT followed by OFT yields a stable increase in SciScore, whereas OFT alone produces no improvement. Without the scientific knowledge base provided by SFT, the model receives two images that are both scientifically incorrect; the preference signal between two poor samples provides insufficient gradient information for meaningful learning.

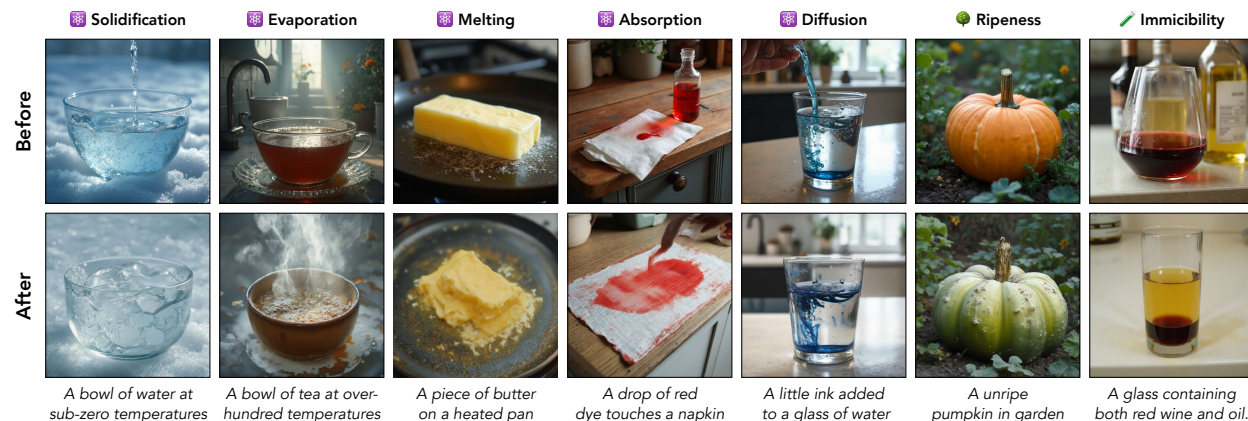


Figure 8: The two-stage framework corrects scientific errors while preserving visual quality. Upper row: base FLUX.1[dev] [14]. Lower row: our fine-tuned model. Each pair uses an identical random seed. Displayed prompts are simplified summaries.

Masking suppresses noise from irrelevant visual features. Starting from the SFT checkpoint, we test two configurations without masking: standard learning rate (yellow curve) and halved learning rate (red curve). At the standard rate, the model collapses because it tries to match all visual features of the preferred image, including irrelevant background elements. Halving the learning rate prevents collapse but fails to increase SciSCORE, as the noisy gradients from irrelevant regions cancel out the useful signal from the scientific region. In contrast, the masked configuration (blue curve) produces a stable and consistent improvement, confirming that restricting gradients to the scientifically relevant region is essential for effective OFT.

6 Related Work

6.1 Scientific Reasoning in Image Generation

A growing body of work investigates whether generative models can adhere to real-world physical laws, spanning image synthesis [17, 58], video generation [19, 20, 59, 60], and 3D modeling [61]. In the image domain, PhyBench [17] introduces a benchmark of physical commonsense tasks and evaluates image generation models through LMM-based scoring. Commonsense-T2I [18] provides paired prompts that test everyday physical reasoning. In the video domain, VideoPhy [19] and PhyGenBench [20] assess whether generated videos obey physical dynamics across material interactions. While these works collectively establish that current models lack scientific reasoning, they share two limitations. First, they are evaluation-only: none provides training data that could be used to improve model capabilities. Second, their evaluation protocols rely on LMM-based discrete scoring, which we find unreliable for fine-grained scientific judgment. Our work addresses both gaps by providing a large-scale adversarial training set alongside the test set, and by developing SciSCORE, a specialized reward model that offers continuous, calibrated scoring for scientific correctness.

6.2 Post-Training Alignment for Diffusion Models

Post-training methods for diffusion models have been explored along several directions. Rejection-sampling approaches such as VersaT2I [62] and DreamSync [63] filter generated outputs to retain higher-quality samples. ReNO [64] optimizes the initial latent noise at inference time using a differentiable objective. More recently, policy-gradient and preference-based methods have been applied directly to the denoising process [50, 65, 66], using reward signals derived from DPO [67] or PPO [68]. These methods share a common assumption: the desired outputs already lie within the pre-trained model’s generative distribution, so optimization amounts to steering the model toward preferred regions of that distribution. This assumption holds for aesthetic or compositional preferences, where the model has already seen relevant visual patterns during pretraining. However, it breaks down for scientific reasoning, where the target phenomena may be entirely absent from the pretraining data. Our framework addresses this by introducing an SFT stage that first exposes the model to scientific visual patterns, followed by online fine-tuning with a domain-specific reward model to optimize for implicit reasoning.

6.3 Benchmarking Image Generation

Standard metrics such as FID [69], IS [70], LPIPS [71], and CLIPScore [72] remain widely used but primarily measure distributional similarity or general text-image alignment. Recent work has introduced richer evaluation paradigms: HPSv2 [28], PickScore [26], and ImageReward [27] capture human aesthetic preferences; VQA-based methods such as VQAScore [73], TIFA [74], VIEScore [75], LLMscore [76], and DSG [77] probe compositional fidelity through question answering; and T2I-CompBench [78] and CLIP-R-Precision [79] target object attributes and spatial relationships.

However, most of these benchmarks focus on visual aesthetics and compositional fidelity rather than scientific correctness. PhyBench [17] and Commonsense-T2I [18] take important steps toward evaluating physical and commonsense reasoning, but they provide only test prompts and rely on discrete LMM-based scoring. We introduce SciSCORE, a reward model that provides continuous, fine-grained scoring specifically calibrated for scientific correctness, and pair it with a large-scale training set to enable both evaluation and model improvement.

7 Conclusion

In this work, we investigate the gap between visual fidelity and scientific realism in image generation. We construct SCIENCE-T2I, an expert-annotated dataset of over 20k adversarial image pairs spanning 16 scientific domains, and use its test set to benchmark 18 recent models. We find that no model scores above 50 out of 100 under implicit scientific prompts, while the same models score roughly 35 points higher when given explicit descriptions of the intended outcome. This confirms that the bottleneck is not in visual rendering but in scientific reasoning.

To address this gap, we develop SciSCORE, a reward model fine-tuned from CLIP-H [22] that surpasses state-of-the-art LMMs and experienced human evaluators by roughly 5 points on our benchmark. Building on SciSCORE, we propose a two-stage alignment framework: supervised fine-tuning first provides the scientific knowledge base, and masked online fine-tuning then refines the model’s implicit reasoning ability using SciSCORE as the reward signal. Applying this framework to FLUX.1[dev] [14] yields over 50% relative improvement, with the fine-tuned model generalizing to complex scenes not seen during training.

Collectively, these results demonstrate that scientific reasoning in image generation is not an inherent limitation of current architectures but a consequence of missing data and misaligned training objectives. We hope that SCIENCE-T2I and SciSCORE will serve as useful resources for future research on grounding generative models in reality.

Acknowledgments

We thank Alistair King for sharing insightful code, which was instrumental in our fine-tuning process. SX also acknowledges support from Open Path AI Foundation, Intel AI SRS, IITP grant funded by the Korean Government (MSIT) (No. RS-2024-00457882, National AI Research Lab Project), Amazon Research Award, and NSF Award IIS-2443404.

References

- [1] James A Ferwerda, Sumanta N Pattanaik, Peter Shirley, and Donald P Greenberg. A model of visual adaptation for realistic image synthesis. In *Proceedings of the 23rd annual conference on Computer graphics and interactive techniques*, pages 249–258, 1996.
- [2] Donald P Greenberg, Kenneth E Torrance, Peter Shirley, James Arvo, Eric Lafortune, James A Ferwerda, Bruce Walter, Ben Trumbore, Sumanta Pattanaik, and Sing-Choong Foo. A framework for realistic image synthesis. In *Proceedings of the 24th annual conference on Computer graphics and interactive techniques*, pages 477–494, 1997.
- [3] Henrik Wann Jensen. *Realistic image synthesis using photon mapping*. AK Peters/crc Press, 2001.
- [4] Han Zhang, Tao Xu, Hongsheng Li, Shaoting Zhang, Xiaogang Wang, Xiao lei Huang, and Dimitris N. Metaxas. Stackgan: Text to photo-realistic image synthesis with stacked generative adversarial networks. In *Proceedings of the IEEE International Conference on Computer Vision (ICCV)*, Oct 2017.

- [5] Wengling Chen and James Hays. Sketchygan: Towards diverse and realistic sketch to image synthesis. In *Proceedings of the IEEE Conference on Computer Vision and Pattern Recognition (CVPR)*, June 2018.
- [6] Han Zhang, Tao Xu, Hongsheng Li, Shaoting Zhang, Xiaogang Wang, Xiaolei Huang, and Dimitris N Metaxas. Stackgan++: Realistic image synthesis with stacked generative adversarial networks. *IEEE transactions on pattern analysis and machine intelligence*, 41(8):1947–1962, 2018.
- [7] Michael F Cohen and John R Wallace. *Radiosity and realistic image synthesis*. Morgan Kaufmann, 1993.
- [8] Dustin Podell, Zion English, Kyle Lacey, Andreas Blattmann, Tim Dockhorn, Jonas Müller, Joe Penna, and Robin Rombach. Sdxl: Improving latent diffusion models for high-resolution image synthesis, 2023. URL <https://arxiv.org/abs/2307.01952>.
- [9] Jiaming Song, Chenlin Meng, and Stefano Ermon. Denoising diffusion implicit models, 2022. URL <https://arxiv.org/abs/2010.02502>.
- [10] Robin Rombach, Andreas Blattmann, Dominik Lorenz, Patrick Esser, and Björn Ommer. High-resolution image synthesis with latent diffusion models, 2022. URL <https://arxiv.org/abs/2112.10752>.
- [11] Liang Chen, Shuai Bai, Wenhao Chai, Weichu Xie, Haozhe Zhao, Leon Vinci, Junyang Lin, and Baobao Chang. Multimodal representation alignment for image generation: Text-image interleaved control is easier than you think. *arXiv preprint arXiv:2502.20172*, 2025.
- [12] Tian Ye, Sixiang Chen, Wenhao Chai, Zhaohu Xing, Jing Qin, Ge Lin, and Lei Zhu. Learning diffusion texture priors for image restoration. In *Proceedings of the IEEE/CVF Conference on Computer Vision and Pattern Recognition*, pages 2524–2534, 2024.
- [13] Shidong Cao, Wenhao Chai, Shengyu Hao, and Gaoang Wang. Image reference-guided fashion design with structure-aware transfer by diffusion models. In *Proceedings of the IEEE/CVF Conference on Computer Vision and Pattern Recognition*, pages 3525–3529, 2023.
- [14] Flux. <https://blackforestlabs.ai/>.
- [15] Dalle-3. <https://openai.com/index/dall-e-3/>.
- [16] Kai Yang, Jian Tao, Jiafei Lyu, Chunjiang Ge, Jiabin Chen, Qimai Li, Weihang Shen, Xiaolong Zhu, and Xiu Li. Using human feedback to fine-tune diffusion models without any reward model, 2024. URL <https://arxiv.org/abs/2311.13231>.
- [17] Fanqing Meng, Wenqi Shao, Lixin Luo, Yahong Wang, Yiran Chen, Quanfeng Lu, Yue Yang, Tianshuo Yang, Kaipeng Zhang, Yu Qiao, et al. Phybench: A physical commonsense benchmark for evaluating text-to-image models. *arXiv preprint arXiv:2406.11802*, 2024.
- [18] Xingyu Fu, Muyu He, Yujie Lu, William Yang Wang, and Dan Roth. Commonsense-t2i challenge: Can text-to-image generation models understand commonsense?, 2024. URL <https://arxiv.org/abs/2406.07546>.
- [19] Hritik Bansal, Zongyu Lin, Tianyi Xie, Zeshun Zong, Michal Yarom, Yonatan Bitton, Chenfanfu Jiang, Yizhou Sun, Kai-Wei Chang, and Aditya Grover. Videophy: Evaluating physical commonsense for video generation. *arXiv preprint arXiv:2406.03520*, 2024.
- [20] Fanqing Meng, Jiaqi Liao, Xinyu Tan, Wenqi Shao, Quanfeng Lu, Kaipeng Zhang, Yu Cheng, Dianqi Li, Yu Qiao, and Ping Luo. Towards world simulator: Crafting physical commonsense-based benchmark for video generation. *arXiv preprint arXiv:2410.05363*, 2024.
- [21] Gpt-4o. <https://openai.com/index/hello-gpt-4o/>.
- [22] Gabriel Ilharco, Mitchell Wortsman, Ross Wightman, Cade Gordon, Nicholas Carlini, Rohan Taori, Achal Dave, Vaishaal Shankar, Hongseok Namkoong, John Miller, Hannaneh Hajishirzi, Ali Farhadi, and Ludwig Schmidt. Openclip, July 2021. URL <https://doi.org/10.5281/zenodo.5143773>. If you use this software, please cite it as below.

- [23] Jia Deng, Wei Dong, Richard Socher, Li-Jia Li, Kai Li, and Li Fei-Fei. Imagenet: A large-scale hierarchical image database. In *2009 IEEE Conference on Computer Vision and Pattern Recognition*, pages 248–255, 2009. doi: 10.1109/CVPR.2009.5206848.
- [24] Alex Krizhevsky. Learning multiple layers of features from tiny images. Technical report, 2009.
- [25] Tsung-Yi Lin, Michael Maire, Serge Belongie, Lubomir Bourdev, Ross Girshick, James Hays, Pietro Perona, Deva Ramanan, C. Lawrence Zitnick, and Piotr Dollár. Microsoft coco: Common objects in context, 2015. URL <https://arxiv.org/abs/1405.0312>.
- [26] Yuval Kirstain, Adam Polyak, Uriel Singer, Shahbuland Matiana, Joe Penna, and Omer Levy. Pick-a-pic: An open dataset of user preferences for text-to-image generation, 2023. URL <https://arxiv.org/abs/2305.01569>.
- [27] Jiazheng Xu, Xiao Liu, Yuchen Wu, Yuxuan Tong, Qinkai Li, Ming Ding, Jie Tang, and Yuxiao Dong. Imagereward: Learning and evaluating human preferences for text-to-image generation. *arXiv preprint arXiv:2304.05977*, 2023.
- [28] Xiaoshi Wu, Yiming Hao, Keqiang Sun, Yixiong Chen, Feng Zhu, Rui Zhao, and Hongsheng Li. Human preference score v2: A solid benchmark for evaluating human preferences of text-to-image synthesis. *arXiv preprint arXiv:2306.09341*, 2023.
- [29] Qwen Team. Qwen3.5: Towards native multimodal agents, February 2026. URL <https://qwen.ai/blog?id=qwen3.5>.
- [30] Meituan LongCat Team, Hanghang Ma, Haoxian Tan, Jiale Huang, Junqiang Wu, Jun-Yan He, Lishuai Gao, Songlin Xiao, Xiaoming Wei, Xiaoqi Ma, Xunliang Cai, Yayong Guan, and Jie Hu. Longcat-image technical report, 2025. URL <https://arxiv.org/abs/2512.07584>.
- [31] Glm-image. <https://github.com/zai-org/GLM-Image>.
- [32] Enze Xie, Junsong Chen, Junyu Chen, Han Cai, Haotian Tang, Yujun Lin, Zhekai Zhang, Muyang Li, Ligeng Zhu, Yao Lu, and Song Han. Sana: Efficient high-resolution image synthesis with linear diffusion transformer, 2024. URL <https://arxiv.org/abs/2410.10629>.
- [33] Qi Qin, Le Zhuo, Yi Xin, Ruoyi Du, Zhen Li, Bin Fu, Yiting Lu, Jiakang Yuan, Xinyue Li, Dongyang Liu, Xiangyang Zhu, Manyuan Zhang, Will Beddow, Erwann Millon, Victor Perez, Wenhai Wang, Conghui He, Bo Zhang, Xiaohong Liu, Hongsheng Li, Yu Qiao, Chang Xu, and Peng Gao. Lumina-image 2.0: A unified and efficient image generative framework, 2025. URL <https://arxiv.org/abs/2503.21758>.
- [34] Patrick Esser, Sumith Kulal, Andreas Blattmann, Rahim Entezari, Jonas Müller, Harry Saini, Yam Levi, Dominik Lorenz, Axel Sauer, Frederic Boesel, Dustin Podell, Tim Dockhorn, Zion English, Kyle Lacey, Alex Goodwin, Yannik Marek, and Robin Rombach. Scaling rectified flow transformers for high-resolution image synthesis, 2024. URL <https://arxiv.org/abs/2403.03206>.
- [35] Image Team, Huanqia Cai, Sihan Cao, Ruoyi Du, Peng Gao, Steven Hoi, Zhaohui Hou, Shijie Huang, Dengyang Jiang, Xin Jin, Liangchen Li, Zhen Li, Zhong-Yu Li, David Liu, Dongyang Liu, Junhan Shi, Qilong Wu, Feng Yu, Chi Zhang, Shifeng Zhang, and Shilin Zhou. Z-image: An efficient image generation foundation model with single-stream diffusion transformer, 2025. URL <https://arxiv.org/abs/2511.22699>.
- [36] Chaorui Deng, Deyao Zhu, Kunchang Li, Chenhui Gou, Feng Li, Zeyu Wang, Shu Zhong, Weihao Yu, Xiaonan Nie, Ziang Song, Guang Shi, and Haoqi Fan. Emerging properties in unified multimodal pretraining, 2025. URL <https://arxiv.org/abs/2505.14683>.
- [37] Black Forest Labs. FLUX.2: Frontier Visual Intelligence. <https://bfl.ai/blog/flux-2>, 2025.
- [38] Chenfei Wu, Jiahao Li, Jingren Zhou, Junyang Lin, Kaiyuan Gao, Kun Yan, Sheng ming Yin, Shuai Bai, Xiao Xu, Yilei Chen, Yuxiang Chen, Zecheng Tang, Zekai Zhang, Zhengyi Wang, An Yang, Bowen Yu, Chen Cheng, Dayiheng Liu, Deqing Li, Hang Zhang, Hao Meng, Hu Wei, Jingyuan Ni, Kai Chen, Kuan Cao, Liang Peng, Lin Qu, Minggang Wu, Peng Wang, Shuting Yu, Tingkun Wen, Wensen Feng, Xiaoxiao Xu, Yi Wang, Yichang Zhang, Yongqiang Zhu, Yujia Wu, Yuxuan Cai, and Zenan Liu. Qwen-image technical report, 2025. URL <https://arxiv.org/abs/2508.02324>.

- [39] Alec Radford, Jong Wook Kim, Chris Hallacy, Aditya Ramesh, Gabriel Goh, Sandhini Agarwal, Girish Sastry, Amanda Askell, Pamela Mishkin, Jack Clark, Gretchen Krueger, and Ilya Sutskever. Learning transferable visual models from natural language supervision, 2021. URL <https://arxiv.org/abs/2103.00020>.
- [40] Ashish Vaswani, Noam Shazeer, Niki Parmar, Jakob Uszkoreit, Llion Jones, Aidan N. Gomez, Lukasz Kaiser, and Illia Polosukhin. Attention is all you need, 2023. URL <https://arxiv.org/abs/1706.03762>.
- [41] Nisan Stiennon, Long Ouyang, Jeff Wu, Daniel M. Ziegler, Ryan Lowe, Chelsea Voss, Alec Radford, Dario Amodei, and Paul Christiano. Learning to summarize from human feedback, 2022. URL <https://arxiv.org/abs/2009.01325>.
- [42] Long Ouyang, Jeff Wu, Xu Jiang, Diogo Almeida, Carroll L. Wainwright, Pamela Mishkin, Chong Zhang, Sandhini Agarwal, Katarina Slama, Alex Ray, John Schulman, Jacob Hilton, Fraser Kelton, Luke Miller, Maddie Simens, Amanda Askell, Peter Welinder, Paul Christiano, Jan Leike, and Ryan Lowe. Training language models to follow instructions with human feedback, 2022. URL <https://arxiv.org/abs/2203.02155>.
- [43] Junnan Li, Dongxu Li, Caiming Xiong, and Steven Hoi. Blip: Bootstrapping language-image pre-training for unified vision-language understanding and generation, 2022. URL <https://arxiv.org/abs/2201.12086>.
- [44] Junnan Li, Dongxu Li, Silvio Savarese, and Steven Hoi. Blip-2: Bootstrapping language-image pre-training with frozen image encoders and large language models, 2023. URL <https://arxiv.org/abs/2301.12597>.
- [45] Xiaohua Zhai, Basil Mustafa, Alexander Kolesnikov, and Lucas Beyer. Sigmoid loss for language image pre-training, 2023. URL <https://arxiv.org/abs/2303.15343>.
- [46] Bo Li, Yuanhan Zhang, Dong Guo, Renrui Zhang, Feng Li, Hao Zhang, Kaichen Zhang, Peiyuan Zhang, Yanwei Li, Ziwei Liu, and Chunyuan Li. Llava-onevision: Easy visual task transfer, 2024. URL <https://arxiv.org/abs/2408.03326>.
- [47] Peng Wang, Shuai Bai, Sinan Tan, Shijie Wang, Zhihao Fan, Jinze Bai, Keqin Chen, Xuejing Liu, Jialin Wang, Wenbin Ge, Yang Fan, Kai Dang, Mengfei Du, Xuancheng Ren, Rui Men, Dayiheng Liu, Chang Zhou, Jingren Zhou, and Junyang Lin. Qwen2-vl: Enhancing vision-language model’s perception of the world at any resolution, 2024. URL <https://arxiv.org/abs/2409.12191>.
- [48] Zhe Chen, Jiannan Wu, Wenhai Wang, Weijie Su, Guo Chen, Sen Xing, Muyan Zhong, Qinglong Zhang, Xizhou Zhu, Lewei Lu, Bin Li, Ping Luo, Tong Lu, Yu Qiao, and Jifeng Dai. Internvl: Scaling up vision foundation models and aligning for generic visual-linguistic tasks, 2024. URL <https://arxiv.org/abs/2312.14238>.
- [49] Jason Wei, Xuezhi Wang, Dale Schuurmans, Maarten Bosma, Brian Ichter, Fei Xia, Ed Chi, Quoc Le, and Denny Zhou. Chain-of-thought prompting elicits reasoning in large language models, 2023. URL <https://arxiv.org/abs/2201.11903>.
- [50] Kevin Black, Michael Janner, Yilun Du, Ilya Kostrikov, and Sergey Levine. Training diffusion models with reinforcement learning, 2024. URL <https://arxiv.org/abs/2305.13301>.
- [51] Ying Fan, Olivia Watkins, Yuqing Du, Hao Liu, Moonkyung Ryu, Craig Boutilier, Pieter Abbeel, Mohammad Ghavamzadeh, Kangwook Lee, and Kimin Lee. Dpok: Reinforcement learning for fine-tuning text-to-image diffusion models, 2023. URL <https://arxiv.org/abs/2305.16381>.
- [52] Bram Wallace, Meihua Dang, Rafael Rafailov, Linqi Zhou, Aaron Lou, Senthil Purushwalkam, Stefano Ermon, Caiming Xiong, Shafiq Joty, and Nikhil Naik. Diffusion model alignment using direct preference optimization, 2023. URL <https://arxiv.org/abs/2311.12908>.
- [53] Yaron Lipman, Ricky T. Q. Chen, Heli Ben-Hamu, Maximilian Nickel, and Matt Le. Flow matching for generative modeling, 2023. URL <https://arxiv.org/abs/2210.02747>.
- [54] Carles Domingo-Enrich, Michal Drozdal, Brian Karrer, and Ricky T. Q. Chen. Adjoint matching: Fine-tuning flow and diffusion generative models with memoryless stochastic optimal control, 2024. URL <https://arxiv.org/abs/2409.08861>.

- [55] Rafael Rafailov, Archit Sharma, Eric Mitchell, Stefano Ermon, Christopher D. Manning, and Chelsea Finn. Direct preference optimization: Your language model is secretly a reward model, 2024. URL <https://arxiv.org/abs/2305.18290>.
- [56] Shilong Liu, Zhaoyang Zeng, Tianhe Ren, Feng Li, Hao Zhang, Jie Yang, Qing Jiang, Chunyuan Li, Jianwei Yang, Hang Su, Jun Zhu, and Lei Zhang. Grounding dino: Marrying dino with grounded pre-training for open-set object detection, 2024. URL <https://arxiv.org/abs/2303.05499>.
- [57] Edward J. Hu, Yelong Shen, Phillip Wallis, Zeyuan Allen-Zhu, Yuanzhi Li, Shean Wang, Lu Wang, and Weizhu Chen. Lora: Low-rank adaptation of large language models, 2021. URL <https://arxiv.org/abs/2106.09685>.
- [58] Yunlong Lin, Tian Ye, Sixiang Chen, Zhenqi Fu, Yingying Wang, Wenhao Chai, Zhaohu Xing, Lei Zhu, and Xinghao Ding. Aglldiff: Guiding diffusion models towards unsupervised training-free real-world low-light image enhancement. *arXiv preprint arXiv:2407.14900*, 2024.
- [59] Bingyi Kang, Yang Yue, Rui Lu, Zhijie Lin, Yang Zhao, Kaixin Wang, Gao Huang, and Jiashi Feng. How far is video generation from world model: A physical law perspective. 2024.
- [60] Wenhao Chai, Xun Guo, Gaoang Wang, and Yan Lu. Stablevideo: Text-driven consistency-aware diffusion video editing. In *Proceedings of the IEEE/CVF International Conference on Computer Vision*, pages 23040–23050, 2023.
- [61] Minghao Guo, Bohan Wang, Pingchuan Ma, Tianyuan Zhang, Crystal Elaine Owens, Chuang Gan, Joshua B Tenenbaum, Kaiming He, and Wojciech Matusik. Physically compatible 3d object modeling from a single image. *arXiv preprint arXiv:2405.20510*, 2024.
- [62] Jianshu Guo, Wenhao Chai, Jie Deng, Hsiang-Wei Huang, Tian Ye, Yichen Xu, Jiawei Zhang, Jenq-Neng Hwang, and Gaoang Wang. Versat2i: Improving text-to-image models with versatile reward. *arXiv preprint arXiv:2403.18493*, 2024.
- [63] Jiao Sun, Deqing Fu, Yushi Hu, Su Wang, Royi Rassin, Da-Cheng Juan, Dana Alon, Charles Herrmann, Sjoerd van Steenkiste, Ranjay Krishna, et al. Dreamsync: Aligning text-to-image generation with image understanding feedback. In *Synthetic Data for Computer Vision Workshop@ CVPR 2024*, 2023.
- [64] Luca Eyring, Shyamgopal Karthik, Karsten Roth, Alexey Dosovitskiy, and Zeynep Akata. Reno: Enhancing one-step text-to-image models through reward-based noise optimization. *arXiv preprint arXiv:2406.04312*, 2024.
- [65] Bram Wallace, Meihua Dang, Rafael Rafailov, Linqi Zhou, Aaron Lou, Senthil Purushwalkam, Stefano Ermon, Caiming Xiong, Shafiq Joty, and Nikhil Naik. Diffusion model alignment using direct preference optimization. In *Proceedings of the IEEE/CVF Conference on Computer Vision and Pattern Recognition*, pages 8228–8238, 2024.
- [66] Kai Yang, Jian Tao, Jiafei Lyu, Chunjiang Ge, Jiabin Chen, Weihang Shen, Xiaolong Zhu, and Xiu Li. Using human feedback to fine-tune diffusion models without any reward model. In *Proceedings of the IEEE/CVF Conference on Computer Vision and Pattern Recognition*, pages 8941–8951, 2024.
- [67] Rafael Rafailov, Archit Sharma, Eric Mitchell, Christopher D Manning, Stefano Ermon, and Chelsea Finn. Direct preference optimization: Your language model is secretly a reward model. *Advances in Neural Information Processing Systems*, 36, 2024.
- [68] John Schulman, Filip Wolski, Prafulla Dhariwal, Alec Radford, and Oleg Klimov. Proximal policy optimization algorithms, 2017. URL <https://arxiv.org/abs/1707.06347>.
- [69] Martin Heusel, Hubert Ramsauer, Thomas Unterthiner, Bernhard Nessler, and Sepp Hochreiter. Gans trained by a two time-scale update rule converge to a local nash equilibrium. *Advances in neural information processing systems*, 30, 2017.
- [70] Tim Salimans, Ian Goodfellow, Wojciech Zaremba, Vicki Cheung, Alec Radford, and Xi Chen. Improved techniques for training gans. *Advances in neural information processing systems*, 29, 2016.

- [71] Richard Zhang, Phillip Isola, Alexei A Efros, Eli Shechtman, and Oliver Wang. The unreasonable effectiveness of deep features as a perceptual metric. In *Proceedings of the IEEE conference on computer vision and pattern recognition*, pages 586–595, 2018.
- [72] Jack Hessel, Ari Holtzman, Maxwell Forbes, Ronan Le Bras, and Yejin Choi. Clipscore: A reference-free evaluation metric for image captioning. *arXiv preprint arXiv:2104.08718*, 2021.
- [73] Baiqi Li, Zhiqiu Lin, Deepak Pathak, Jiayao Li, Yixin Fei, Kewen Wu, Xide Xia, Pengchuan Zhang, Graham Neubig, and Deva Ramanan. Evaluating and improving compositional text-to-visual generation. In *Proceedings of the IEEE/CVF Conference on Computer Vision and Pattern Recognition*, pages 5290–5301, 2024.
- [74] Yushi Hu, Benlin Liu, Jungo Kasai, Yizhong Wang, Mari Ostendorf, Ranjay Krishna, and Noah A Smith. Tifa: Accurate and interpretable text-to-image faithfulness evaluation with question answering. *arXiv preprint arXiv:2303.11897*, 2023.
- [75] Max Ku, Dongfu Jiang, Cong Wei, Xiang Yue, and Wenhui Chen. Viescore: Towards explainable metrics for conditional image synthesis evaluation. *arXiv preprint arXiv:2312.14867*, 2023.
- [76] Yujie Lu, Xianjun Yang, Xiujun Li, Xin Eric Wang, and William Yang Wang. Llmscore: Unveiling the power of large language models in text-to-image synthesis evaluation. *arXiv preprint arXiv:2305.11116*, 2023.
- [77] Jaemin Cho, Yushi Hu, Roopal Garg, Peter Anderson, Ranjay Krishna, Jason Baldridge, Mohit Bansal, Jordi Pont-Tuset, and Su Wang. Davidsonian scene graph: Improving reliability in fine-grained evaluation for text-image generation. *arXiv preprint arXiv:2310.18235*, 2023.
- [78] Kaiyi Huang, Kaiyue Sun, Enze Xie, Zhenguo Li, and Xihui Liu. T2i-compbench: A comprehensive benchmark for open-world compositional text-to-image generation. In *Thirty-seventh Conference on Neural Information Processing Systems Datasets and Benchmarks Track*, 2023.
- [79] Dong Huk Park, Samaneh Azadi, Xihui Liu, Trevor Darrell, and Anna Rohrbach. Benchmark for compositional text-to-image synthesis. In *Thirty-fifth Conference on Neural Information Processing Systems Datasets and Benchmarks Track (Round 1)*, 2021.
- [80] Hany Farid. Perspective (in)consistency of paint by text, 2022. URL <https://arxiv.org/abs/2206.14617>.
- [81] Ayush Sarkar, Hanlin Mai, Amitabh Mahapatra, Svetlana Lazebnik, D. A. Forsyth, and Anand Bhattad. Shadows don't lie and lines can't bend! generative models don't know projective geometry...for now, 2024. URL <https://arxiv.org/abs/2311.17138>.
- [82] Ic-light. <https://openreview.net/pdf?id=u1cQYxRI1H>.
- [83] Ziwei Huang, Wanggui He, Quanyu Long, Yandi Wang, Haoyuan Li, Zhelun Yu, Fangxun Shu, Long Chan, Hao Jiang, Leilei Gan, and Fei Wu. T2i-factualbench: Benchmarking the factuality of text-to-image models with knowledge-intensive concepts, 2024. URL <https://arxiv.org/abs/2412.04300>.
- [84] Ilya Loshchilov and Frank Hutter. Decoupled weight decay regularization, 2019. URL <https://arxiv.org/abs/1711.05101>.
- [85] Tero Karras, Miika Aittala, Timo Aila, and Samuli Laine. Elucidating the design space of diffusion-based generative models, 2022. URL <https://arxiv.org/abs/2206.00364>.
- [86] Diederik P Kingma and Max Welling. Auto-encoding variational bayes, 2022. URL <https://arxiv.org/abs/1312.6114>.
- [87] Laion-aesthetics. <https://laion.ai/blog/laion-aesthetics/>.

Appendix

The Appendix is structured as follows:

- Section **A**: why we restrict tasks to linguistically describable phenomena, and why tasks such as reflections and shadows are excluded.
- Section **B**: definitions and visual contrasts for all 16 tasks, organized by Biology, Chemistry, and Physics.
- Section **C**: the subject + condition decomposition that underlies ST/CT classification, with the full task assignment.
- Section **D**: three-stage data curation pipeline covering prompt generation, image synthesis, and quality control.
- Section **E**: a comparison of SCIENCE-T2I with existing scientific and commonsense reasoning benchmarks.
- Section **F**: hyper-parameters for training SciSCORE.
- Section **G**: evaluation protocol and setup for VLM, LMM, and human baselines.
- Section **H**: per-category accuracy breakdowns on both test splits, revealing where SciSCORE achieves perfect accuracy and where it struggles.
- Section **I**: analysis of why VLMs approach random guessing, why LMMs fail despite CoT, and why SciSCORE surpasses human evaluators.
- Section **J**: qualitative examples showing how IEE improves fine-grained visual discrimination.
- Section **K**: mathematical derivations for SFT, DPO, noise scheduling, subject extraction, and gradient masking.
- Section **L**: hyper-parameter configurations for both the SFT and OFT stages.
- Section **M**: additional OFT experiments using LAION aesthetic and ImageReward as alternative reward models.
- Section **N**: discussion of cross-task generalizability limitations and subject-oriented task challenges.

A Why We Prioritize Linguistically Describable Tasks

A natural question when designing SCIENCE-T2I is why we restrict the task set to phenomena whose visual outcomes can be fully described through text. During the design process, we considered several additional reasoning categories that would broaden scientific coverage. For instance, reflection-based tasks [80] evaluate whether objects and their mirror reflections are geometrically consistent, and shadow-based tasks [81] test whether cast shadows follow the correct light-source geometry.

However, we find that these tasks present a fundamental obstacle for our adversarial data curation pipeline. Both correct and incorrect versions of a reflection or shadow require precise control over geometric details that cannot be specified through text alone. Current image generation models lack the spatial precision to reliably produce such controlled pairs, making it impossible to construct the tuples that SCIENCE-T2I relies on for preference modeling.

This observation leads to a deliberate design principle: every task in SCIENCE-T2I must satisfy the *rewriting capability* requirement, meaning that the scientific visual outcome can be unambiguously expressed through an alternative textual description. For example, “an unripe apple” can be rewritten as “a green apple,” preserving the intended visual meaning. This property guarantees that (1) explicit and superficial prompt variants can be derived from any implicit prompt, and (2) image generation models can interpret and produce the target images reliably. Tasks involving geometric or lighting precision beyond the reach of textual prompts, such as reflections [80] and subtle illumination effects [82], remain important directions for future work as generation models improve in spatial control.

B Task Definitions and Visual Contrasts

Each of the 16 tasks in SCIENCE-T2I targets a specific scientific phenomenon and defines the visual contrast that the model must reason about. We organize them by scientific domain below. Illustrative examples from the dataset are shown in Figures 20, 21, and 22.

- **Light Requirement (LR)**: Plants change color and leaf size depending on whether they receive adequate or insufficient light.

Task Category	Task Name	Count
Subject-oriented Task	Immiscibility	218
	Flame Reaction	206
	Buoyancy	204
	Diffusion	142
	Absorption	160
Condition-oriented Task	Rust	288
	Light Requirement	201
	Water Requirement	201
	Liquidation	195
	Electricity	186
	Solidification	117
	Melting	192
	Gravity	221
	Evaporation	183
	Ripeness	192
Seasonal Change	240	

Figure 9: Subject-oriented vs. condition-oriented task classification. Ten of the 16 tasks in SCIENCE-T2I are condition-oriented and six are subject-oriented. Condition-oriented tasks involve generalizable visual patterns, while subject-oriented tasks require subject-specific scientific knowledge.

- **Watering Requirement (WR):** Plants exhibit differences in foliage health and growth under sufficient versus inadequate watering, with the latter causing wilting and reduced leaf size.
- **Ripeness (RI):** Fruits alter their color and texture when ripe compared to unripe.
- **Seasonal Change (SC):** Plants display variations in leaf color, size, and blooming patterns across seasons.
- **Flame Reaction (FR):** Chemical substances produce characteristic flame colors when burned.
- **Immiscibility (IM):** Two liquids either mix uniformly or separate into visible layers based on chemical properties.
- **Rust (RU):** Metals appear shiny and reflective before oxidation, and corroded, flaky, and discolored after rusting.
- **Absorption (AB):** A solid either absorbs a liquid or repels it, depending on their material properties.
- **Buoyancy (BU):** Objects either float on or sink in water based on their density relative to water.
- **Diffusion (DI):** A small amount of liquid added to another either disperses uniformly or remains separate.
- **Electricity (EL):** Electronic devices change appearance (e.g., glowing, sparking) when electric current is applied versus disconnected.
- **Evaporation (EV):** Liquids boil and produce vapor upon reaching boiling point; below it, the surface remains calm.
- **Gravity (GR):** Objects appear differently positioned under normal gravity versus a gravity-free environment.
- **Liquidation (LI):** Air condenses into water droplets on surfaces cooled below room temperature.
- **Melting (ME):** Solids transition to liquid, changing shape and structure upon reaching their melting point.
- **Solidification (SO):** Liquids become solids, altering form and texture when cooled below their solidification point.

C All Tasks Follow a Subject + Condition Structure

We observe that every task in SCIENCE-T2I can be decomposed into a **subject** and a **condition**. For example, the prompt *an unripe apple* comprises the subject *apple* and the condition *unripe*; *a laptop without electricity* includes the subject *laptop* and the condition *without electricity*. This uniform structure motivates a two-way classification based on *where* the scientific reasoning lies: in the subject or in the condition.

Subject-oriented tasks. In these tasks, the need for scientific reasoning arises from the subject’s intrinsic properties. Different subjects under the same condition exhibit different visual features. For example, the *buoyancy* task is subject-oriented because whether an object floats or sinks depends on its density relative to water, an intrinsic property that varies across subjects. Other subject-oriented tasks include *flame reaction* (different metals produce different flame colors), *immiscibility*, *absorption*, *diffusion*, and *electricity*.

Condition-oriented tasks. In these tasks, the scientific reasoning is tied to the applied condition. Varying subjects under a single condition produce similar visual outcomes. For instance, the *gravity* task is condition-oriented because most subjects behave similarly: floating in zero gravity and resting on the ground under normal gravity. The remaining condition-oriented tasks include *ripeness*, *seasonal change*, *light requirement*, *watering requirement*, *rust*, *evaporation*, *liquidation*, *melting*, and *solidification*.

User Prompt

Assume you are an experienced scientist. Your task is to generate both an explicit prompt and a superficial prompt based on a given input prompt. The input prompt is formulated with scientific principles and will serve as input for a text-to-image generative model. It may include terminology or phrases that are not overtly descriptive but imply certain visual characteristics or phenomena, requiring interpretative scientific reasoning to convey their meaning.

Explicit Prompt: Reformulate the input prompt into a precise, descriptively accurate statement that aligns with the intended visual outcome, incorporating the implied scientific nuances.

Superficial Prompt: Construct an interpretation that disregards the underlying scientific reasoning. Focus only on the superficial or literal descriptive aspects.

Example: {"input prompt": "an unripe apple", "explicit prompt": "a green apple", "superficial prompt": "a red apple"}

Here is the input prompt: [Your Input]. Please output in the following format:

```
{"explicit prompt": , "superficial prompt": }
```

Figure 10: Instruction template for prompt generation. Given an implicit prompt, GPT-4o [21] generates the corresponding explicit and superficial prompts.

Why this distinction matters. As shown in Figure 9, ten tasks are condition-oriented and six are subject-oriented. This classification proves analytically useful: as we demonstrate in Section 4.4, nearly all failure cases of SciSCORE concentrate in subject-oriented tasks, where the model must have prior exposure to each subject’s specific properties. Condition-oriented tasks, by contrast, involve generalizable visual patterns that transfer more easily across subjects.

D Data Curation Pipeline: Prompts, Images, and Quality Control

In this section, we describe the three stages of our data curation pipeline in detail.

Stage 1: prompt generation. For each of the 16 tasks, we use GPT-4o [21] to define a set of structured templates for implicit prompts. These templates capture the core scientific principle while allowing variability in the objects or substances involved. Using these templates, GPT-4o generates a diverse set of implicit prompts by inserting appropriate subjects. For each implicit prompt, GPT-4o then produces the corresponding explicit and superficial prompts following the instruction template shown in Figure 10. This three-stage process (template → implicit → explicit/superficial) ensures that all three prompt types within a tuple remain semantically aligned while differing precisely in their level of scientific specificity.

Stage 2: image synthesis. Images relevant to our scientific reasoning tasks are scarce in existing datasets. We therefore generate synthetic images, selecting the generation model based on two criteria:

- **Text-image alignment.** The model must accurately render both explicit and superficial prompts, as faithful alignment is essential for constructing valid adversarial pairs. Misalignment at this stage would introduce label noise into the training set.
- **Photorealistic style.** Because our tasks are grounded in real-world phenomena, the generated images must exhibit a photorealistic style. Abstract or stylized renderings would obscure the fine-grained visual differences that distinguish scientifically correct from incorrect images.

We compare SDXL [8], SD 3 [34], DALLE 3 [15], and FLUX.1[dev] [14] on a representative subset of prompts. As shown in Figure 11, FLUX.1[dev] consistently produces the most faithful and realistic outputs across all task categories. We therefore adopt FLUX.1[dev] for all image generation in SCIENCE-T2I.

Stage 3: quality control. The scientific principles embedded in each implicit prompt manifest as specific visual features in localized regions of the image (e.g., the color of a flame, the surface texture of a rusted metal). During curation, we focus on ensuring these regions accurately reflect the underlying science. We apply two filtering criteria:

- **Background simplicity.** We select images with minimal background complexity (e.g., solid colors) to eliminate distracting visual elements that could confound the scientific signal.

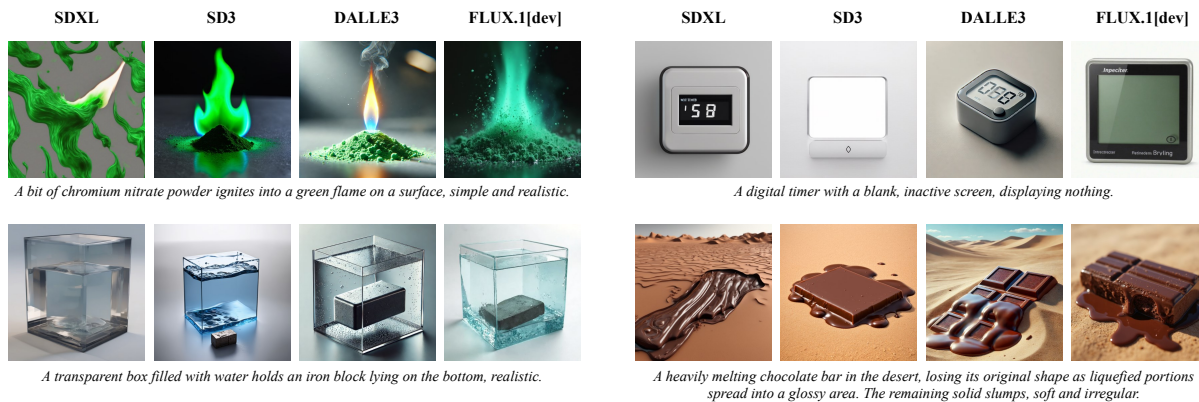


Figure 11: FLUX.1[dev] produces the most faithful and realistic images among compared models. SDXL [8], SD 3 [34], and DALLE 3 [15] occasionally fail to align generated images with the provided descriptions, while FLUX.1[dev] [14] consistently renders accurate content with photorealistic quality.

- **Region prominence.** We filter to ensure that the scientifically relevant region occupies a large portion of the image, maximizing the visual salience of the target phenomenon.

Representative examples of curated images are shown in Figures 20, 21, and 22. All generated tuples undergo a final round of manual verification by domain experts, who cross-reference each image against established scientific knowledge to confirm correctness.

E SCIENCE-T2I Unifies Training and Dual-Purpose Evaluation

Table 5 compares SCIENCE-T2I with existing benchmarks targeting physical or commonsense reasoning in image generation. Most prior benchmarks provide only test prompts and support only one evaluation mode. In contrast, SCIENCE-T2I is designed around two complementary capabilities.

First, SCIENCE-T2I includes a training set of over 20k adversarial pairs, enabling both reward model training and generative model alignment. To our knowledge, none of the existing benchmarks in this space provides a training set. Second, the test set supports two distinct evaluation modes within a single framework. On one hand, it benchmarks the scientific reasoning of image generation models by scoring their outputs under implicit prompts (Section 3). On the other hand, the same test set evaluates the scientific judgment of LMMs and VLMs through a two-choice selection task that tests whether these models can distinguish scientifically correct images from incorrect ones (Section 4.4). This dual-purpose design allows researchers to assess both generation and understanding capabilities using the same prompts and grading criteria, eliminating the need for separate benchmarks.

Table 5: SCIENCE-T2I is the only benchmark that provides a training set and supports both generation and LMM evaluation. Existing benchmarks offer test-only evaluation for a single task type, while SCIENCE-T2I unifies training data, generation benchmarking, and LMM evaluation in one package.

Benchmark	Type	Category	Training Set	Evaluation	
				Generation	LMM
Commonsense-T2I [18]	Commonsense	5	✗	✓	✗
T2I-FactualBench [83]	Commonsense	8	✗	✓	✗
PhyBench [17]	Science	31	✗	✓	✗
SCIENCE-T2I (Ours)	Science	16	✓	✓	✓

LMM Evaluation Instruction

You will be presented with a textual prompt followed by two visual images. Your task is to critically analyze and compare both images, selecting the one that most accurately aligns with and represents the overall meaning of the given prompt. **First, you should imagine how an ideal image would look based on the prompt, and then describe both images in detail. Finally, combining your initial visualization with the descriptions of the two images, you should select the image that most effectively conveys the intended meaning of the prompt, providing a reasoned justification for your choice.**

Input: {"prompt": [Your Input Prompt], "image-1": [Your Input Image], "image-2": [Your Input Image]}

Output format:

{'imagination': , 'description of image-1': , 'description of image-2': , 'justification for choice': , 'final choice': }

Figure 12: LMM evaluation instruction. Red text indicates additional fields used for CoT [49] reasoning.

F Training Settings for SciSCORE

Table 6 summarizes the hyper-parameters used to train SciSCORE.

Table 6: Hyper-parameters for training SciSCORE.

Hyper-parameters	SciSCORE
batch size	128
learning rate	2×10^{-6}
learning rate schedule	cosine
weight decay	0.3
training steps	600
warmup steps	150
optimizer	AdamW [84]
λ	0.25

G Baseline Setup and Evaluation Process for SciSCORE

Evaluation protocol. Each evaluation instance presents one implicit prompt alongside two images: one generated from the explicit prompt and one from the superficial prompt. Models and human evaluators are asked to select the image that better corresponds to the implicit prompt.

Vision-language models (VLMs). We evaluate CLIP-H [22], BLIP-2 [44], and SigLIP [45]. For each model, we encode the implicit prompt and both images using their respective text and image encoders, then apply the scoring mechanism described in Section 4.1 to select the higher-scoring image.

Large multimodal models (LMMs). We evaluate LLaVA-OV [46], Qwen2-VL [47], InternVL [48], and GPT-4o-mini [21]. For GPT-4o-mini, we test both a standard setting and a CoT setting [49] that encourages step-by-step reasoning. Each LMM is prompted to choose between two images. To mitigate order bias, we evaluate each pair twice with reversed image order and average the accuracy. The full instruction template is shown in Figure 12.

Human evaluation. We recruit 10 evaluators, all holding at least a bachelor’s degree in science or engineering. Unlike the dataset curators, who verify accuracy using scientific literature, the evaluators rely solely on their own knowledge to select the better image. This distinction explains why human performance, while strong, is not perfect.

H Per-Category Results of SciSCORE

Tables 7 and 8 break down the results from Table 2 by individual task category. Abbreviations follow the definitions in Appendix B. SciSCORE achieves perfect accuracy (100%) on multiple tasks across both splits, while its failures concentrate in subject-oriented tasks such as Buoyancy (BU) and Immiscibility (IM), where fine-grained subject-specific knowledge is required.

Table 7: SciScore achieves perfect accuracy on most tasks in SCIENCE-T2I-S. Per-category accuracy (%). Green highlights the best VLM; blue highlights the best LMM.

Model	ME	DI	EL	SO	IM	EV	AB	LI	FR	SC	RI	RU	LR	WR	BU	GR
CLIP-H [22]	25.00	71.43	47.62	40.48	54.17	26.67	57.14	77.78	73.33	81.48	34.62	16.67	62.22	31.11	63.89	78.33
BLIPScore [43]	56.94	50.00	52.38	44.05	53.12	20.00	38.10	33.33	76.67	58.33	38.46	42.86	76.67	38.89	50.00	47.50
SigLIP ViT-SO-14 [45]	44.44	83.33	47.62	45.24	60.42	63.33	57.14	58.33	62.22	83.33	53.85	23.81	46.67	33.33	58.33	78.33
LLaVA-OV-7B [46]	36.11	75.00	77.38	55.95	55.21	100.00	38.10	95.83	48.89	78.70	46.15	59.52	51.11	72.22	45.83	92.50
Qwen2-VL-7B [47]	26.39	70.24	77.38	42.86	66.67	68.33	40.48	84.72	52.22	95.37	34.62	73.81	57.78	67.78	47.22	83.33
InternVL2.5-8B [48]	41.67	63.10	72.62	52.38	56.25	91.67	47.62	90.28	52.22	84.26	75.00	69.05	84.44	90.00	55.56	96.67
GPT-4o mini	36.11	77.38	82.14	35.71	65.63	100.00	33.33	76.39	58.89	97.22	53.85	95.24	96.67	83.33	56.94	71.31
GPT-4o mini+ CoT [49]	36.11	85.71	86.90	45.24	68.75	100.00	33.33	81.94	56.67	98.15	61.54	97.62	96.67	88.89	52.78	80.33
Human Eval	98.15	65.87	95.63	86.11	77.78	100.00	66.67	82.08	80.95	90.74	94.62	92.86	96.89	99.56	74.55	92.99
SciScore (ours)	100.00	97.62	100.00	90.48	68.75	100.00	71.43	100.00	97.78	100.00	100.00	100.00	100.00	100.00	100.00	98.33

Table 8: SciScore maintains strong per-category performance on SCIENCE-T2I-C despite complex backgrounds. Per-category accuracy (%). Green highlights the best VLM; blue highlights the best LMM.

Model	ME	DI	EL	SO	IM	EV	AB	LI	FR	SC	RI	RU	LR	WR	BU	GR
CLIP-H [22]	66.67	78.57	21.43	57.14	50.00	0.00	64.29	66.67	46.67	88.89	75.00	35.71	80.00	60.00	58.33	75.00
BLIPScore [43]	58.33	50.00	28.57	42.86	62.50	50.00	50.00	29.17	60.00	75.00	54.17	57.14	53.33	46.67	62.50	40.00
SigLIP ViT-SO-14 [45]	58.33	85.71	42.86	42.86	62.50	30.00	64.29	41.67	60.00	94.44	83.33	28.57	46.67	53.33	66.67	95.00
LLaVA-OV-7B [46]	45.83	71.43	64.29	71.43	59.38	100.00	57.14	79.17	36.67	77.78	79.17	53.57	63.33	86.67	75.00	100.00
Qwen2-VL-7B [47]	41.67	64.29	67.86	57.14	53.13	55.00	57.14	70.83	36.67	94.44	75.00	60.71	93.33	96.67	66.67	100.00
InternVL2.5-8B [48]	58.33	92.86	57.14	53.57	71.88	95.00	57.14	70.83	50.00	75.00	87.50	75.00	90.00	93.33	75.00	97.50
GPT-4o mini	67.65	67.86	64.29	50.00	68.75	90.00	50.00	75.00	53.33	88.89	87.50	89.29	100.00	83.33	54.17	97.50
GPT-4o mini+ CoT [49]	67.65	85.71	85.71	57.14	68.75	95.00	32.14	79.17	50.00	88.89	87.50	92.86	100.00	93.33	41.67	100.00
Human Eval	91.03	66.75	90.87	77.55	86.61	95.71	78.57	76.79	77.14	96.83	83.78	92.86	88.57	84.76	83.33	98.57
SciScore (ours)	100.00	85.71	85.71	92.86	81.25	100.00	71.43	100.00	100.00	100.00	100.00	92.86	100.00	100.00	41.67	100.00

I Analysis of VLM, LMM, and Human Performance

We provide further analysis of the results in Section 4.4.

VLM performance approaches random guessing. As shown by the ROC curves in Figure 14, the AUC scores of CLIP-H [22], BLIPScore [43], and SigLIP [45] are only marginally above 0.5, confirming near-random performance. We attribute this to the nature of CLIP-style pretraining: the text encoder learns to match descriptive surface-level terms with visual content. When presented with an implicit prompt and two images that both contain the described subject, the model cannot distinguish between the scientifically correct and incorrect versions because the distinguishing features are not captured by the text-image alignment objective. In contrast, SciScore achieves a near-perfect AUC, demonstrating strong discriminative power.

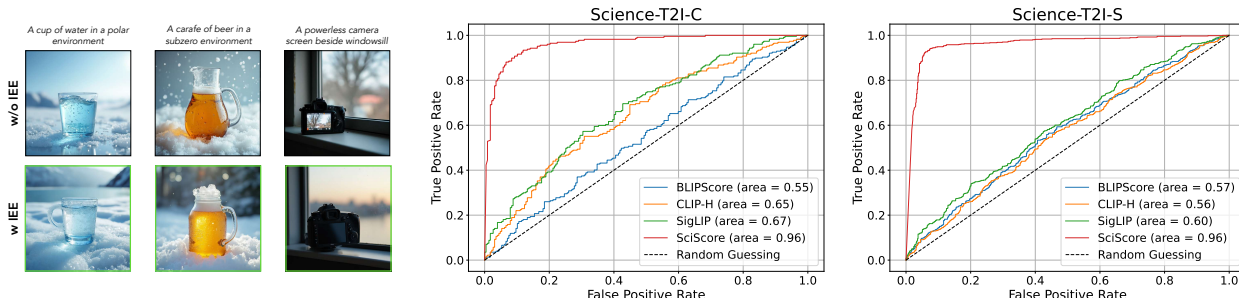


Figure 13: Qualitative Results of

IEE. Images enclosed by green borders denote the correct selection in each pair. Figure 14: SciScore achieves near-perfect AUC while VLMS hover near 0.5. ROC curves for CLIP-H, BLIPScore, SigLIP, and SciScore.

LMMs struggle with visual scientific reasoning. Despite access to extensive knowledge bases, all LMMs including GPT-4o-mini [21] underperform on our benchmark, even with CoT prompting [49]. We identify two primary failure modes, illustrated in Figure 18. First, the models often misinterpret fine-grained visual features critical to scientific tasks, such as subtle color differences or spatial relationships between objects. Second, even when visual perception is adequate, the models produce internally contradictory reasoning chains, undermining the reliability of their final judgments. These observations suggest that the bottleneck lies in visual perception and reasoning coherence rather than knowledge availability.

Why SciSCORE surpasses human evaluators. Human evaluators possess broad but finite scientific knowledge. Their expertise is inevitably bounded by their specific training backgrounds, which can lead to errors on tasks outside their immediate domain. SciSCORE, by contrast, acquires task-specific knowledge from the SCIENCE-T2I training set and applies it consistently across all domains, explaining its roughly 5% advantage over human evaluators.

J Qualitative Analysis of IEE

Figure 13 illustrates the effect of IEE on SciSCORE’s ability to capture fine-grained visual details. The first two examples involve distinguishing between frozen and liquid states, which requires detecting subtle differences in transparency. The third example requires identifying whether a small screen region displays meaningful content. Without IEE ($\lambda = 0$), the model fails on these cases because the image encoder lacks sensitivity to such fine-grained differences. With IEE ($\lambda = 0.25$), the enhanced image encoder correctly identifies the distinguishing features, confirming that IEE strengthens the model’s visual discrimination at the level required for scientific assessment.

K Details of Two-Stage Training

We provide the full mathematical derivations underlying our two-stage alignment framework.

Supervised Fine-tuning (SFT). Flow matching models [53] are continuous-time generative models that define a time-dependent velocity field $v(x_t, t)$ to transport samples from a noise distribution p_1 to data distribution p_0 over a time interval $t \in [0, 1]$. The transformation is governed by the ordinary differential equation (ODE):

$$\frac{dx_t}{dt} = v(x_t, t), \quad (20)$$

with the initial condition $x_1 \sim p_1$. The forward process is constructed as:

$$x_t = \alpha_t x_0 + \beta_t \epsilon, \quad \epsilon \sim \mathcal{N}(0, I), \quad (21)$$

where $\alpha_0 = 1, \beta_0 = 0, \alpha_1 = 0$, and $\beta_1 = 1$, ensuring the consistency of the marginal distributions with the initial and terminal conditions. The velocity field $v(x_t, t)$ is represented as the sum of two conditional expectations:

$$v(x, t) = \dot{\alpha}_t \mathbb{E}[x_* | x_t = x] + \dot{\beta}_t \mathbb{E}[\epsilon | x_t = x], \quad (22)$$

which can be approximated by the model $v_\theta(x, t)$ by minimizing the following training objective:

$$\mathcal{L}_{SFT}(\theta) := \mathbb{E}_{x_*, \epsilon, t} [\|v_\theta(x_t, t) - \dot{\alpha}_t x_* - \dot{\beta}_t \epsilon\|^2] \quad (23)$$

Direct Preference Optimization (DPO). RLHF aims to optimize a conditional distribution $p_\theta(x_0|c)$ such that the expected reward $r(c, x_0)$ is maximized, while simultaneously regularizing the KL-divergence from a reference distribution p_{ref} . This objective is formulated as:

$$\max_{\theta} \mathbb{E}_{c, x_0 \sim p_\theta(x_0|c)} [r(c, x_0)] - \beta \mathcal{D}_{\text{KL}} [p_\theta(x_0|c) \| p_{\text{ref}}(x_0|c)] \quad (24)$$

where the hyper-parameter β controls regularization. According to [55], the unique global optimal solution p_θ^* to this optimization problem is given by:

$$p_\theta^*(x_0|c) = p_{\text{ref}}(x_0|c) \exp\left(\frac{r(c, x_0)}{\beta}\right) / Z(c) \quad (25)$$

where $Z(c) = \sum_{x_0} p_{\text{ref}}(x_0|c) \exp\left(\frac{r(c, x_0)}{\beta}\right)$ is the partition function. Then the reward function can be expressed as:

$$r(c, x_0) = \beta \log \frac{p_{\theta}^*(x_0|c)}{p_{\text{ref}}(x_0|c)} + \beta \log Z(c) \quad (26)$$

To model human preferences, the Bradley-Terry (BT) model is employed, which represents the probability of one outcome being preferred over another as:

$$p_{BT}(x_0^w \succ x_0^l|c) = \sigma(r(c, x_0^w) - r(c, x_0^l)) \quad (27)$$

where σ is the sigmoid function, x_0^w is the preferred outcome, and x_0^l is the less preferred one. $r(c, x_0)$ can be parameterized by a neural network ϕ and estimated via maximum likelihood training for binary classification:

$$L_{BT}(\phi) = \mathbb{E}_{c, x_0^w, x_0^l} [\log \sigma(r_{\phi}(c, x_0^l) - r_{\phi}(c, x_0^w))] \quad (28)$$

By leveraging the relationship between the reward function and the optimal policy p_{θ}^* , the DPO objective is derived as:

$$\mathcal{L}_{\text{DPO}}(\theta) = -\mathbb{E}_{c, x_0^w, x_0^l} \left[\log \sigma \left(\beta \log \frac{p_{\theta}(x_0^w|c)}{p_{\text{ref}}(x_0^w|c)} - \beta \log \frac{p_{\theta}(x_0^l|c)}{p_{\text{ref}}(x_0^l|c)} \right) \right] \quad (29)$$

Choice of σ_t . We determine the value of σ_t by adhering to the methodology presented in [85]. Initially, we define the hyperparameters S_{churn} , S_{min} , S_{max} , and S_{noise} . Subsequently, we define γ_t as follows:

$$\gamma_t = \begin{cases} \min(S_{\text{churn}} \cdot \Delta t, \sqrt{2} - 1) & \text{if } t \in [S_{\text{min}}, S_{\text{max}}] \\ 0 & \text{otherwise,} \end{cases} \quad (30)$$

where Δt represents the timestep difference between consecutive sampling steps. Following this, we define σ_t by

$$\sigma_t = S_{\text{noise}} \cdot \sqrt{\gamma_t^2 + 2\gamma_t \cdot (1 - t)}. \quad (31)$$

Subject extraction. Before training begins, we use an LLM to extract the subject from each prompt. During OFT, the extracted subjects are passed to GroundingDINO [56] to produce bounding-box masks for each generated image.

Gradient masking in latent space. GroundingDINO produces masks at RGB resolution, but gradients are computed in the model’s latent space. Because the pretrained VAE [86] used by LDM [10] preserves spatial locality, we map the bounding box directly. Let the latent have dimensions (H_l, W_l, C_l) and the decoded image (H, W, C) . A bounding box (x_1, y_1, x_2, y_2) in pixel space maps to:

$$\left(\frac{x_1}{H} \cdot H_l, \frac{y_1}{W} \cdot W_l, \frac{x_2}{H} \cdot H_l, \frac{y_2}{W} \cdot W_l \right) \quad (32)$$

This latent-space mask is applied to the gradients during backpropagation.

Mask padding. For tasks where positional relationships matter (e.g., an object’s height relative to the ground in the *gravity* task), the tight bounding box around the subject is insufficient. We therefore pad the mask by 10% in both height and width to capture the surrounding spatial context.

L Two-Stage Training Settings

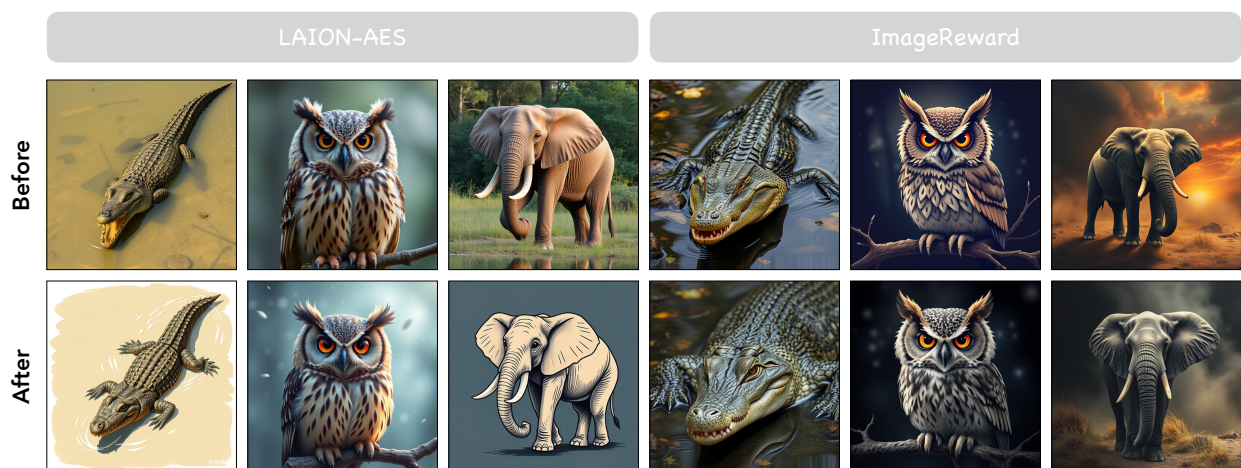
Table 9 lists the hyper-parameter configurations for both SFT and OFT stages.

M Additional Results of Online Fine-tuning

To verify that our OFT pipeline generalizes beyond SCIScore, we conduct additional experiments using two alternative reward models: the LAION aesthetic predictor [87] and ImageReward [27]. In these experiments, we do not apply the masking strategy from the main text, as the tasks (animal generation) do not require subject-level localization.

Table 9: Hyper-parameters for the two-stage alignment framework.

Hyper-parameters	SFT	OFT
batch size	32	8
learning rate	2×10^{-5}	3×10^{-4}
training steps	900	140
optimizer	AdamW [84]	AdamW [84]
gradient accumulation	8	2
LoRA rank	16	16
S_{churn}	/	0.1
$S_{\text{min}}, S_{\text{max}}$	/	$0, \infty$
S_{noise}	/	1.0
β	/	10

**Figure 15: OFT improves visual quality with alternative reward models. Upper: base FLUX.1[schnell] [14]. Lower: after OFT. Each pair uses an identical random seed. Prompts: “crocodile”, “owl”, “elephant.”**

Training. We fine-tune FLUX.1[schnell] [14] with 4 inference steps. All other configurations follow Table 9 except: 128 images per step, learning rate 6×10^{-5} , gradient accumulation of 8. We train for 164 steps with LAION and 550 steps with ImageReward. Following DDPO [50], the training set comprises 45 animal categories.

Evaluation. The test set consists of 10 held-out animal categories. For each prompt, we generate 100 images and report the average reward. Results are shown in Table 10; qualitative examples are provided in Figure 15.

Table 10: OFT consistently improves rewards with alternative reward models. Average reward on 10 held-out animal categories.

Method	LAION [87]	ImageReward [27]
FLUX.1[schnell] [14]	5.855	0.949
+OFT	6.074	1.023

! N Limitations and Future Directions

Limited cross-task generalizability. Scientific knowledge does not transfer easily across domains: expertise in dynamics does not inherently facilitate reasoning about thermodynamics, even for humans. As a result, our alignment framework improves performance primarily on the 16 predefined tasks, and extending it to new scientific domains would require additional domain-specific training data.

Subject-oriented tasks remain difficult. As discussed in Section 4.4, subject-oriented tasks pose the greatest challenge because they require knowledge of each subject’s specific properties. When the model encounters a novel or unseen subject, it lacks the prior exposure needed to generate the correct visual features. Incorporating world knowledge from LLMs or scaling up the training data to cover a broader range of subjects are promising directions for future work.

Grading Criteria Examples

Example 1

Prompt: “A transparent water-filled box holds a basketball, depicted realistically.”

Scene Grading:

- *0 point:* The picture does not feature a basketball inside a transparent box filled with water in any capacity.
- *1 point:* The picture shows a basketball, but it is not inside a transparent box. Alternatively, the basketball are in a transparent box, but there is no water present.
- *2 points:* The picture accurately depicts a basketball inside a transparent box filled with water.

Reality Grading:

- *0 point:* The basketball is completely sinking to the bottom of the water.
- *1–2 points:* The basketball is completely submerging in the water, but doesn’t reach the bottom. Less mistakes will earn a higher score.
- *3 points:* The picture shows basketball floating on the surface of the water.

Example 2

Prompt: “A clear glass filled with water and oil, simple and realistic.”

Scene Grading:

- *0 point:* There is no glass or no liquid in the glass, or the scene is irrelevant (e.g., the focus is not on the glass or liquid at all).
- *1 point:* The glass contains liquid, but the focus on the liquid or the glass is unclear, or there are distracting elements in the scene.
- *2 points:* The glass is clearly depicted with some liquid in it, with no distractions, offering a simple, clear, and realistic depiction.

Reality Grading:

- *0 points:* Liquids are mixed or incorrectly positioned (e.g., water and oil blended or misplaced).
- *1 point:* Water and oil are present but with partial inaccuracies in separation or positioning (e.g., water floating on oil, blurred boundaries).
- *2 points:* Liquids are correctly positioned with visible separation (oil atop water), but minor deviations from realism exist (e.g., slight issues with clarity or texture).
- *3 points:* Fully realistic depiction with correct positioning (oil floating on water) and clear separation.

Figure 16: Representative grading criteria for two tasks. Each tuple specifies the Scene Score rubric (whether the main subject is present) and the Reality Score rubric (whether the scientific phenomenon is correctly depicted).


Evaluation Instruction

You are an experienced scientist. Begin by evaluating the provided image using the specified scene composition criteria. If the image does not fully satisfy these criteria, assign a reality score of 0. However, if the scene meets all the criteria, proceed to assess its realism based on the given reality scoring guidelines, disregarding stylistic aspects and minor background details. Please first describe the image in detail and then adhere strictly to these criteria to ensure an accurate scoring of the image.

Input: {“Prompt”: [Your Input Prompt], “Scene Grading”: [Your Input Scene Grading], “Reality Grading”: [Your Input Reality Grading], “Image”: [Your Input Image]}.

Output format: {“description”: , “scene score”: , “reality score”: }

Figure 17: Instruction template for image evaluation. The evaluator receives an image, its implicit prompt, and the corresponding grading criteria, then produces Scene Score (SS) and Reality Score (RS).



A powerless night light on the nightstand

Which one better aligns with and represents the overall meaning of the given prompt


Imagination: An ideal image would depict a nightstand with a vintage or modern night light that **uses battery power or candles since there's no electricity...**

Description of #1 image: The image shows a lamp with a round white bulb... and **lacks any visible lighting effect...**

Description of #2 image: The image features a warm, glowing lamp with a soft, rounded top, **emitting a gentle orange light...**

Justification for choice: Image #2 most accurately aligns with the prompt as it effectively **conveys the concept of a night light without explicitly needing electricity...**

Final choice: **the second image**



Copper carbonate burns on the tray

Which one better aligns with and represents the overall meaning of the given prompt


Imagination: A small mound of copper carbonate powder on a tray with flames realistically igniting from it. The flames should have a **warm, orange-yellow hue...**

Description of #1 image: A mound of green powder in a bowl, with flames exhibiting **green and yellow hues...**

Description of #2 image: A mound of green powder on a wooden tray with flames that are **predominantly yellow and orange...**

Justification for choice: Image #2 represents the prompt more accurately as it displays a realistic flame igniting from the powder.

Final choice: **the second image**



A bowl of beer in subzero environment

Which one better aligns with and represents the overall meaning of the given prompt

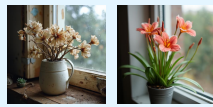
Imagination: An image showing a clear bowl filled with beer, surrounded by a snowy landscape, with **beads of condensation on the outside of the bowl...**

Description of #1 image: The first image features a glass bowl filled with an amber beer sitting on a bed of snow...

Description of #2 image: There's a glass bowl of beer, but it is topped with a substantial mound of icy snow, **making the beer seem partially frozen...**

Justification for choice: The first image more accurately captures the prompt's intent by **effectively highlighting the beer in a realistic outdoor snowy setting...**

Final choice: **the first image**



A rarely watered sapanoria by window

Which one better aligns with and represents the overall meaning of the given prompt

Imagination: An ideal image would **portray a healthy, vibrant sapanoria plant**, ideally situated on a windowsill bathed in natural light...


Description of #1 image: This image shows a **worn ceramic pitcher containing a bouquet of dried flowers, which have a pale and faded appearance...**

Description of #2 image: This image features a potted plant with multiple large, **bright coral-colored flowers and green leaves. The plant appears healthy...**

Justification for choice: Image #2 most accurately reflects the essence of the prompt...

Final choice: **the second image**

(a) Reasoning Failure. GPT-4o-mini [21] inaccurately infers the target image by misinterpreting the input prompt and neglecting the underlying scientific principles embedded within it. Instead of employing a systematic reasoning process, it relies predominantly on intuitive imagination.



A ginkgo tree in spring

Which one better aligns with and represents the overall meaning of the given prompt


Imagination: An ideal image of a ginkgo tree in spring would feature a vibrant tree with **bright green leaves that reflect the freshness of spring...**

Description of #1 image: This image depicts a **ginkgo tree with striking golden-yellow leaves, set against a clearer sky filled with scattered clouds.**

Description of #2 image: This image features a **large tree with bright yellow foliage and a sturdy black trunk...**

Justification for choice: The first image better aligns with the prompt's request **due to the vibrant golden-yellow leaves representing the seasonal transition...**

Final choice: **the first image**



A volleyball in a box filled with water

Which one better aligns with and represents the overall meaning of the given prompt

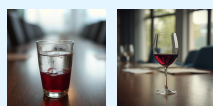
Imagination: An ideal image would depict a transparent box filled with clear water, showcasing a **vibrant volleyball floating inside it...**

Description of #1 image: A transparent box filled with clear water contains a colored volleyball. **The volleyball appears to be slightly floating within the water...**

Description of #2 image: The second image also features a transparent box filled with water. **The volleyball is fully submerged, with only its upper half visible...**

Justification for choice: The first image best represents the prompt because it **floats engagingly in the water...**

Final choice: **the first image**



A glass filled with red wine and mineral oil

Which one better aligns with and represents the overall meaning of the given prompt


Imagination: An image showing a clear glass filled with a **distinct layer of red wine and mineral oil...**

Description of #1 image: The glass is clear and filled with a reddish liquid, but there is **no visible layer of mineral oil...**

Description of #2 image: The glass is clear and filled with a **rich red liquid, showing a darker color with a cleaner look compared to image #1...**

Justification for choice: Neither image accurately represents the prompt, as **both lack the distinct layering of red wine and mineral oil...**

Final choice: **the second image**



A laptop in a box filled with water

Which one better aligns with and represents the overall meaning of the given prompt

Imagination: An ideal image would depict a clear, transparent box filled with water. Inside, **a laptop would be partially submerged, with clear water around it.**

Description of #1 image: This image shows a transparent box filled with clear blue water, **containing a laptop that appears to be partially submerged.**

Description of #2 image: In this image, a transparent box is also filled with clear blue water, but the **laptop appears more submerged compared to the first image.**

Justification for choice: The first image is chosen as it more effectively aligns with the prompt...

Final choice: **the first image**

(b) Visual Limitation. GPT-4o-mini [21] inaccurately describes the image, thereby impeding the reasoning process. Specifically, for tasks involving spatial relationships, it fails to make correct judgments, resulting in erroneous interpretations of positional dynamics within the visual content.

Figure 18: Qualitative Failure Cases of GPT. In both cases, the CoT [49] reasoning approach from Figure 12 is applied, but errors in either interpretation or visual comprehension impact the final decision. Green text indicates correct inference, while red text marks errors.

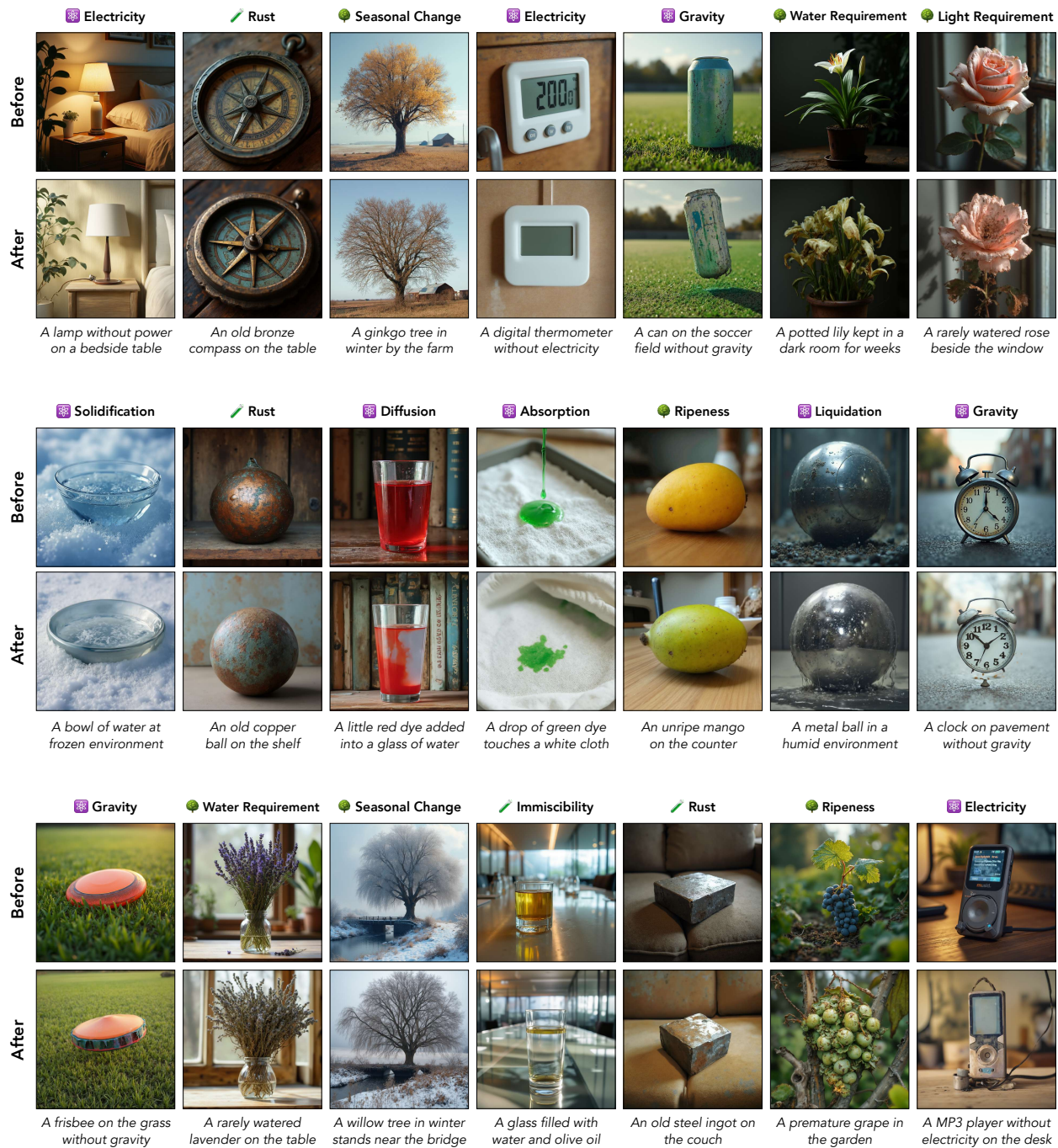


Figure 19: Additional Generated Samples. Each pair of images is produced using the same random seed to ensure consistency.

<p>Buoyancy</p> <p>IP</p> <p>A transparent water-filled box holds an {apple} in a simple and empty background, depicted realistically.</p>			<p>A transparent box filled with water holds an {apple} floating on the surface, realistic. The background is completely empty.</p> <p>EP</p>
<p></p>	<p></p>	<p></p>	<p>A transparent box filled with water holds a submerged {apple}, realistic. The background is completely empty.</p> <p>SP</p>
<p>Diffusion</p> <p>IP</p> <p>A little bit {orange dye} added to a glass of water, simple and realistic.</p>			<p>A bit of {orange dye} spreads and diffuses into the glass of water, in a simple and realistic way.</p> <p>EP</p>
<p></p>	<p></p>	<p></p>	<p>A glass filled with {orange} water, presented in a straightforward and realistic way.</p> <p>SP</p>
<p>Gravity</p> <p>IP</p> <p>A {pillow} in a simple space without gravity, simple and realistic.</p>			<p>A realistic scene of a {pillow} floating in the air within a simple space. The background is completely empty.</p> <p>EP</p>
<p></p>	<p></p>	<p></p>	<p>A realistic scene of a {pillow} lying on the ground within a simple space. The background is completely empty.</p> <p>SP</p>
<p>Melting</p> <p>IP</p> <p>A {butter stick} on a heated pan, simple and realistic.</p>			<p>A heavily melting {butter stick} on a heated pan, losing its original shape as liquefied portions spread into a glossy area.</p> <p>EP</p>
<p></p>	<p></p>	<p></p>	<p>A solid {butter stick} on a heated pan, it remains firm with sharp edges and a stable shape, crafting a simple and realistic scene.</p> <p>SP</p>
<p>Flame Reaction</p> <p>IP</p> <p>A bit of {copper} powder ignites on a surface, in a simple and realistic way.</p>			<p>A bit of {copper} powder ignites into a {green} flame on a surface, the scene simple and realistic.</p> <p>EP</p>
<p></p>	<p></p>	<p></p>	<p>A bit of {copper} powder ignites into a {green} flame on a surface, the scene simple and realistic.</p> <p>SP</p>
<p>Immiscibility</p> <p>IP</p> <p>A clear glass filled with {milk and oil}, simple and realistic.</p>			<p>A clean and distinct separation of layers is visible in the glass, with {milk} at the bottom and {oil} floating on top.</p> <p>EP</p>
<p></p>	<p></p>	<p></p>	<p>A clear glass filled with {oil/milk}, straightforward and realistic.</p> <p>SP</p>

Figure 20: Several examples from SCIENCE-T2I. 'EP' denotes explicit prompts (yellow blocks), 'SP' denotes superficial prompts (blue blocks), and 'IP' denotes implicit prompts (grey blocks).



Figure 21: Several examples from SCIENCE-T2I. 'EP' denotes explicit prompts (yellow blocks), 'SP' denotes superficial prompts (blue blocks), and 'IP' denotes implicit prompts (grey blocks).

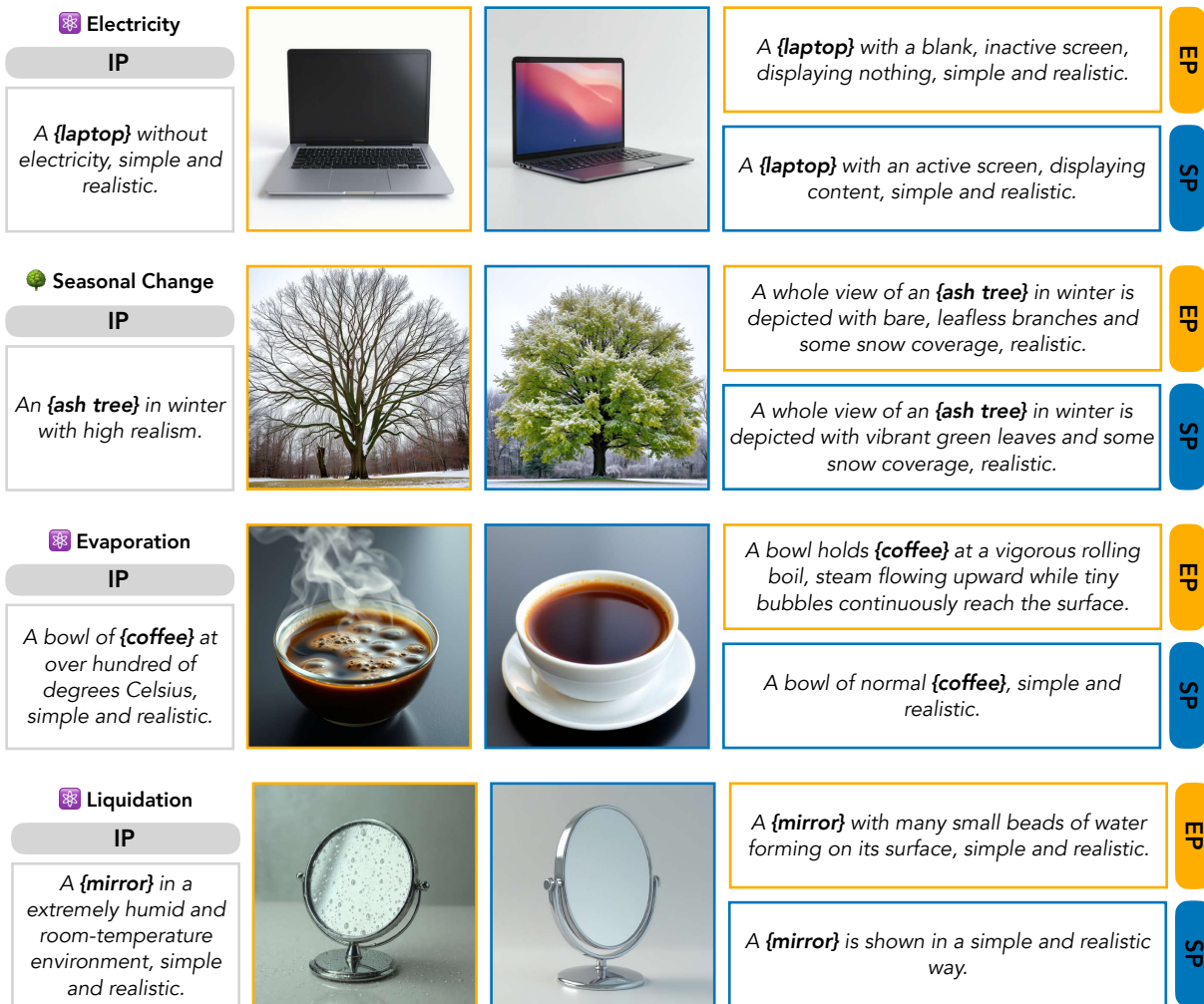


Figure 22: Several examples from SCIENCE-T2I. 'EP' denotes explicit prompts (yellow blocks), 'SP' denotes superficial prompts (blue blocks), and 'IP' denotes implicit prompts (grey blocks).